Electronic Supplementary Material (ESI) for Chemical Science.

Supporting Information

The Unprecedented Strong Paratropic Ring Current of a bis-Pd^{II} Complex of 5,10,23-Trimesityl [28]Heptaphyrin(1.1.0.0.1.0.0)

Yang Liu, Ling Xu, Xiaorong Jin, Bangshao Yin, Yutao Rao, Mingbo Zhou, Jianxin Song*, and Atsuhiro Osuka

Table of Contents

Instruments and Materials

Compound ^{1}H NMR (500 MHz) spectra were taken on a Bruker AVANCE-500 spectrometer, and chemical shifts were reported as the delta scale in ppm relative to $CHCl_3$ as internal reference for ^{1}H NMR (δ = 7.260 ppm). UV/Vis absorption spectra were recorded on a Shimadzu UV-3600 spectrometer. MALDI-TOF mass spectra were obtained with a Bruker ultrafle Xtreme MALDI-TOF/TOF spectrometer with matrix. X-Ray data were taken on an Agilent Supernova X-Ray diffractometer equipped with a large area CCD detector. Redox potentials were measured by cyclic voltammetry on a CHI900 scanning electrochemical microscope. α,α'-Dipyrrol-2-yl BODIPY **1** was prepared by the method of Jiao and Hao's report.[1] α,α'-Dibromotripyrrin **2** was prepared by the method of Tanaka's report.[2] Unless otherwise noted, chemicals obtained from commercial suppliers were used without further purification.

General Procedures and Compound Data

Synthesis of **3**:

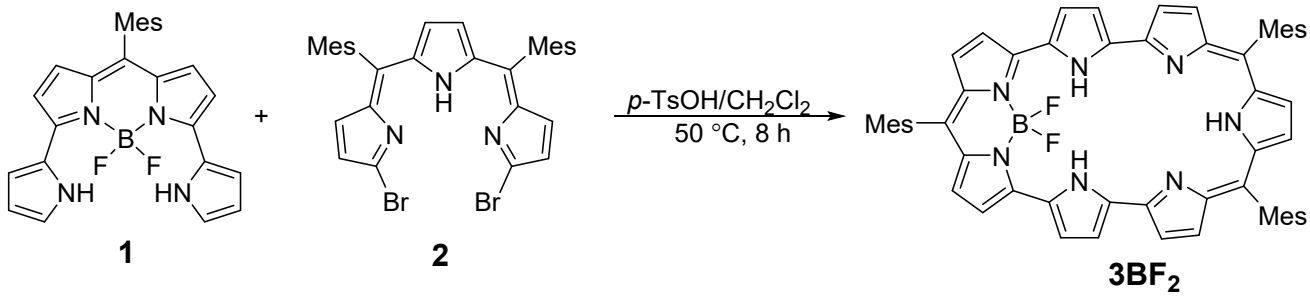

A flask containing **1** (399.2 mg, 1.0 mmol), **2**[S1] (615.4 mg, 1.0 mmol), *p*-TsOH (172.2 mg, 1.0 mmol) was purged with argon, and then charged with dry CH_2Cl_2 (50 mL). The resulting mixture was stirred at 50°C for 8 h. The reaction mixture was passed through a short Al_2O_3 column to remove polymeric materials. After the solvent was evaporated in vacuo, the product was separated by Al_2O_3 column chromatography with CH_2Cl_2/*n*-hexane as an eluent. Recrystallization with CH_2Cl_2/MeOH gave **3BF$_2$** (204 mg, 23 % yield) as brown solids.

3BF$_2$: ^{1}H NMR (500 MHz, $CDCl_3$, 298 K) δ = 6.72 (s, 2H, Ar-H), 6.65 (m, 4H, Ar-H), 5.42 (d, J = 3.7 Hz, 2H, β-H), 5.39−5.35 (m, 6H, β-H), 5.12 (d, J = 3.5 Hz, 2H, β-H), 4.98 (d, J = 3.5 Hz, 2H, β-H), 4.79 (s, 2H, β-H), 2.19 (m, 9H, Me-H), 2.15 (s, 6H, Me-H) and 2.07 (s, 12H, Me-H) ppm; NH protons were not observed at room tempearture.

1H NMR (500 MHz, $CDCl_3$, 213 K) δ = 18.18 (s, 2H, NH), 17.73 (s, 1H, NH), 6.69 (s, 2H, Ar-H), 6.63 (s, 4H, Ar-H), 5.33 (br, 2H, β-H), 5.27 (s, 4H, β-H), 5.21 (br, 2H, β-H), 4.99 (br, 2H, β-H), 4.86 (br, 2H, β-H), 4.75 (br, 2H, β-H), 2.15 (br, 9H, Me-H), 2.13 (s, 6H, Me-H) and 2.03 (s, 12H, Me-H) ppm.

^{13}C NMR (126 MHz, $CDCl_3$) δ = 166.7, 156.4, 143.1, 140.8, 140.4, 138.6, 138.0, 137.2, 136.3, 135.7, 135.5, 132.1, 128.7, 128.2, 128.0, 127.4, 123.9, 119.7, 119.3, 20.9 and 19.4 ppm; HR-MS (MALDI-TOF-MS): *m/z* = 893.4298, calcd for $(C_{58}H_{50}BF_2N_7)^+$ = 893.4233 ($[M]^+$); λ_{max} (ε [$M^{-1}cm^{-1}$]) = 311(15700), 464 (63600), 524 (59900) and 740 (2800) nm.

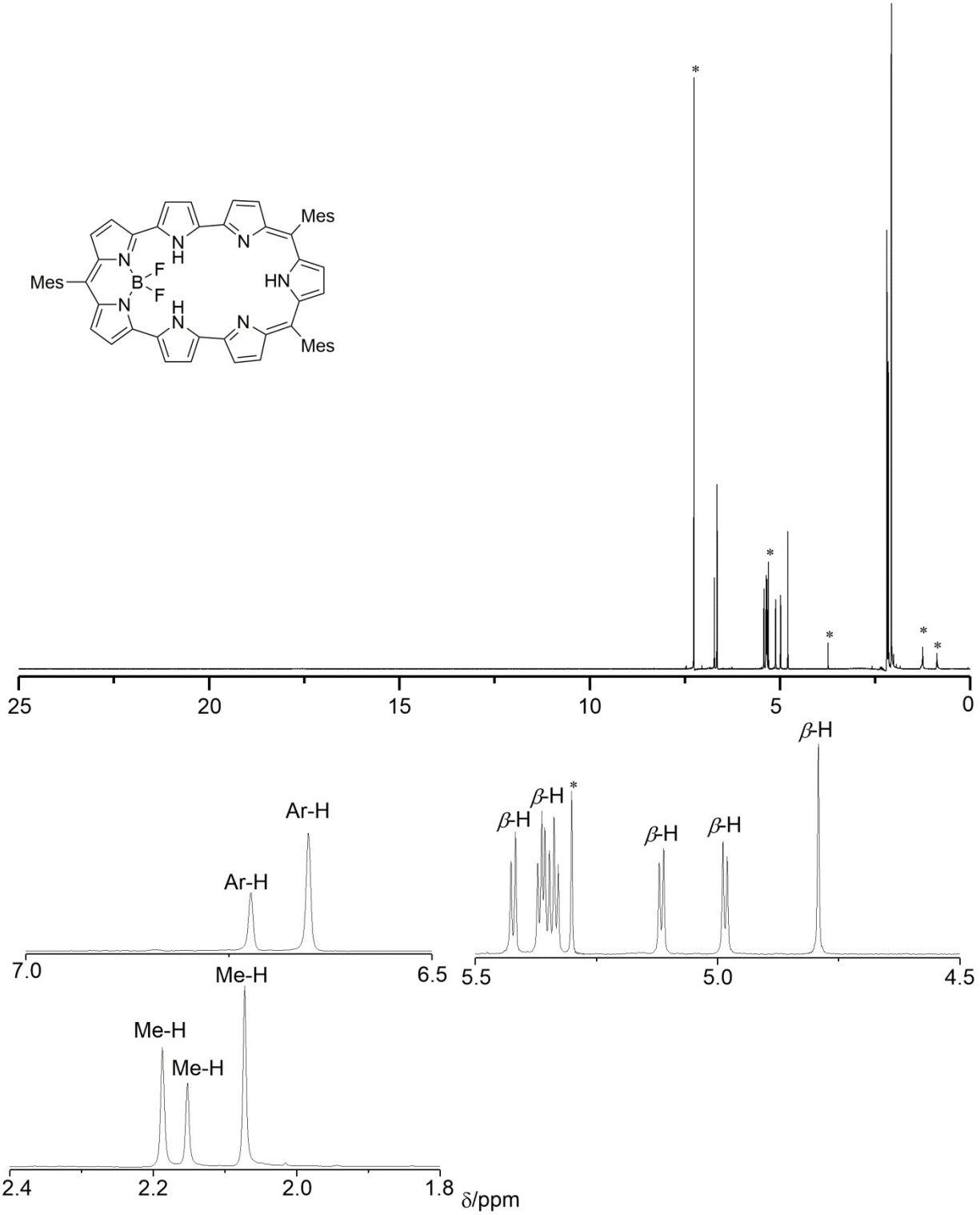

Figure S1.[1]H NMR spectrum of **$3BF_2$** in $CDCl_3$ at 298 K. Asterisk means residual solvent or impurity.

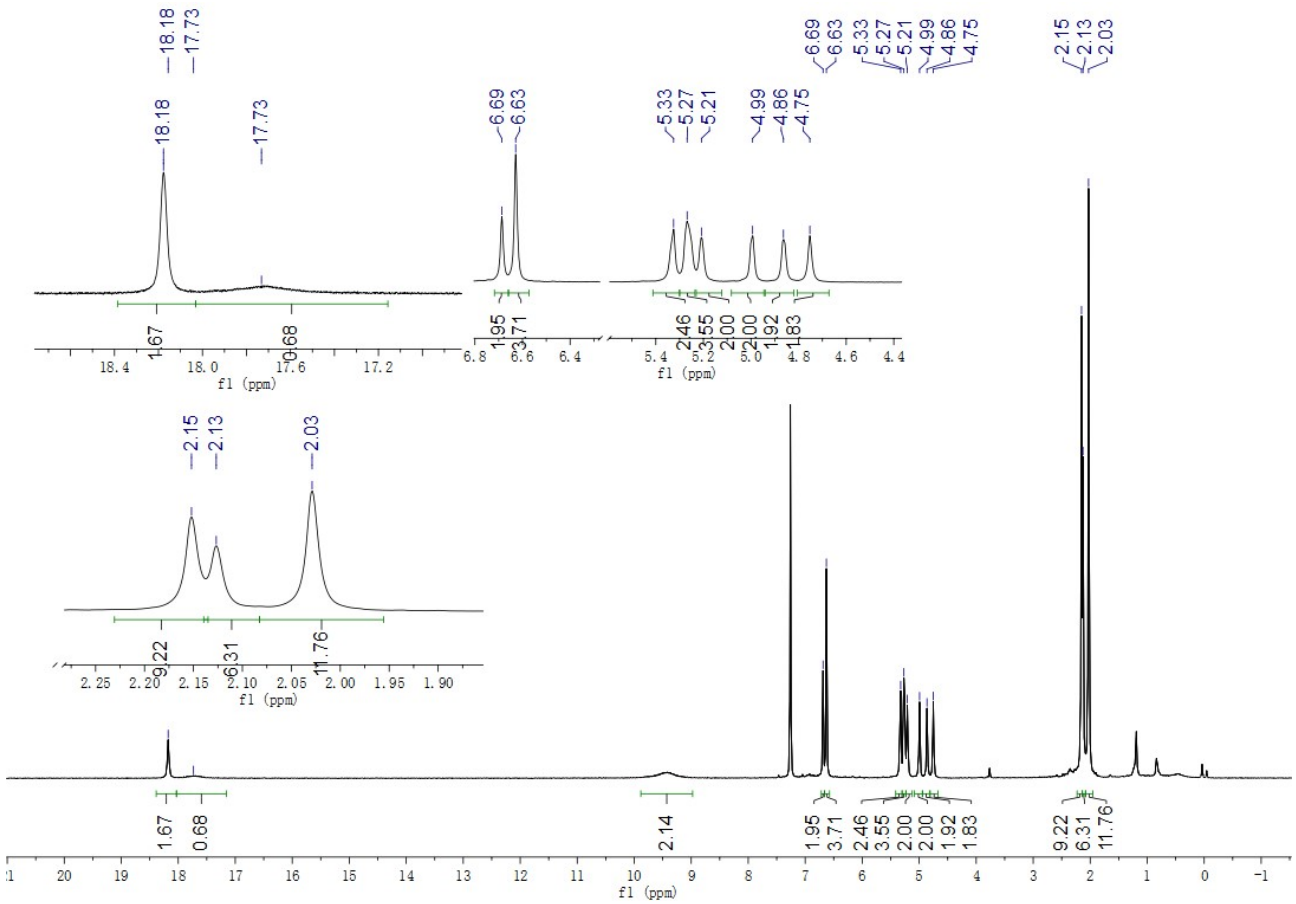

Figure S2.[1]H NMR spectrum of **$3BF_2$** in $CDCl_3$ at 213 K.

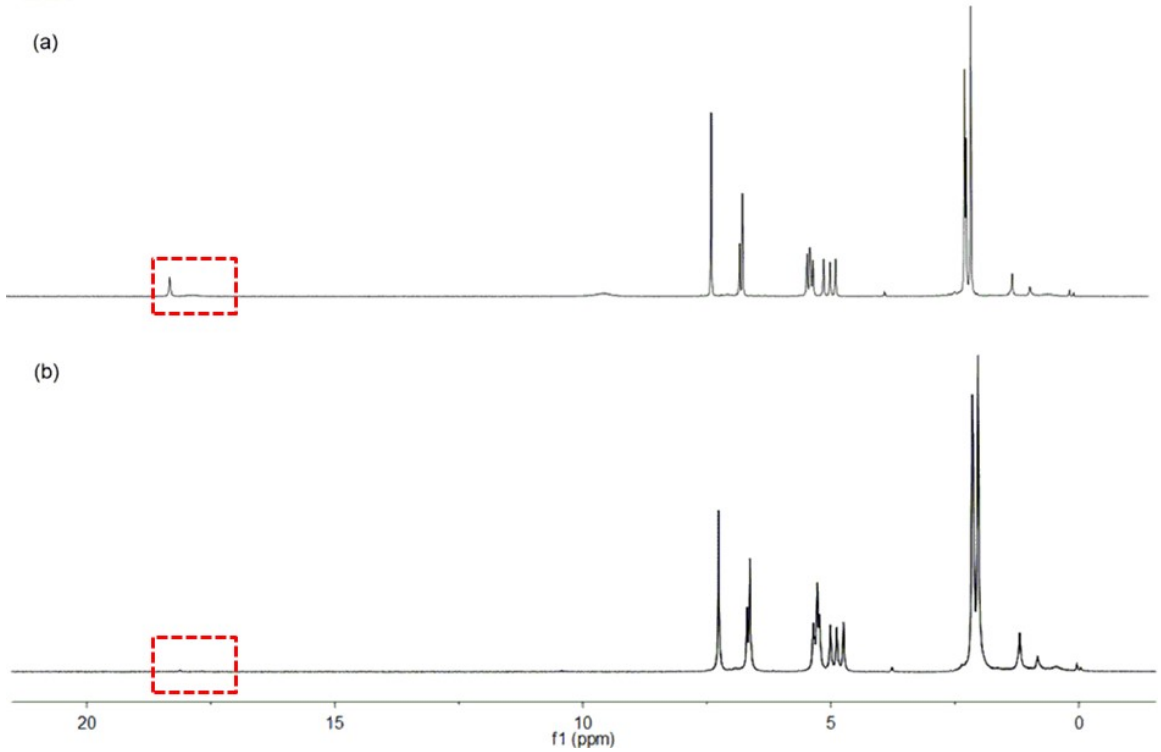

Figure S3.[1]H NMR spectra of **$3BF_2$**; (a) at 213 K in $CDCl_3$ and (b) with D_2O.

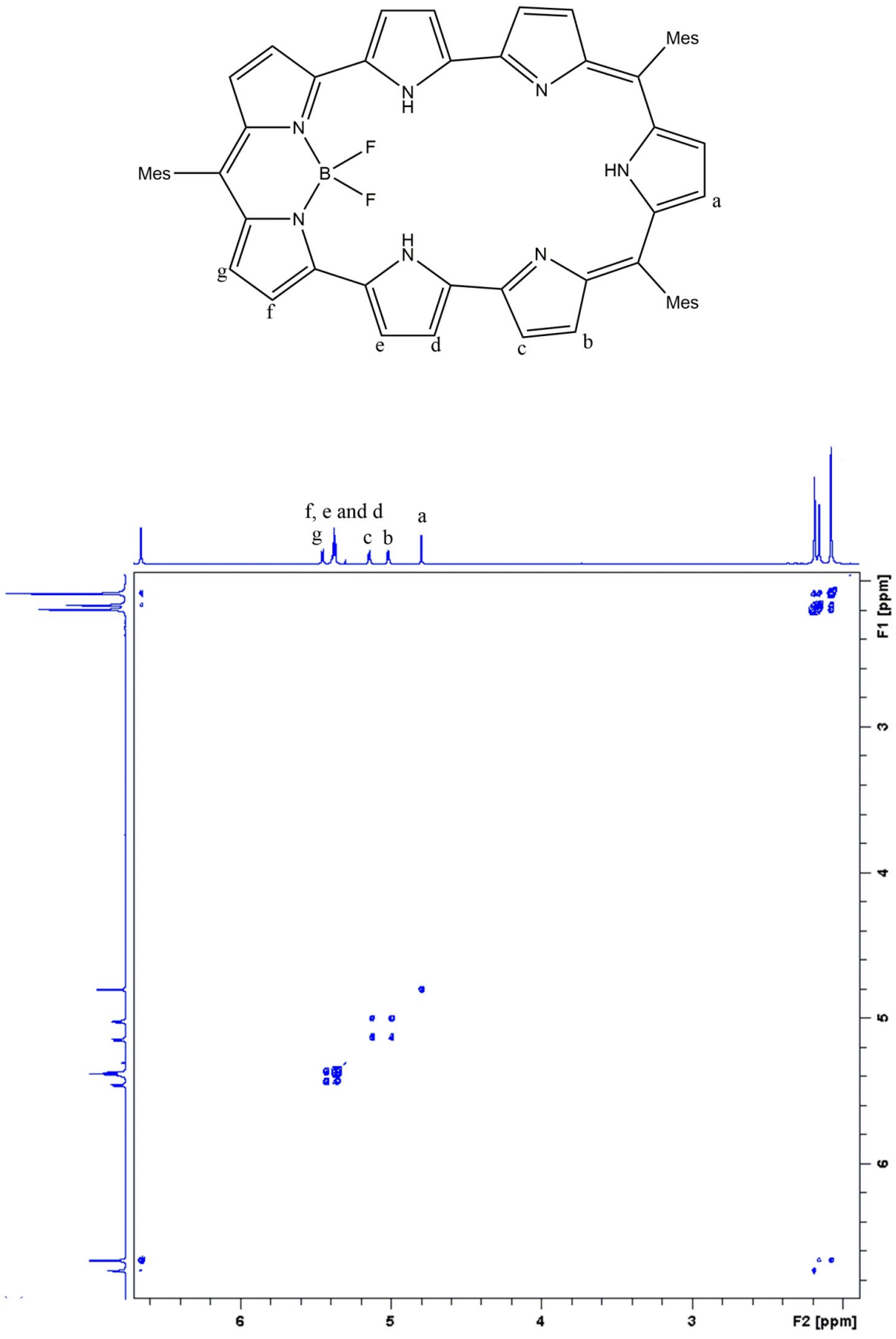

Figure S4. ^{1}H-^{1}H COSY spectrum of **3BF$_2$** in $CDCl_3$ at 298 K.

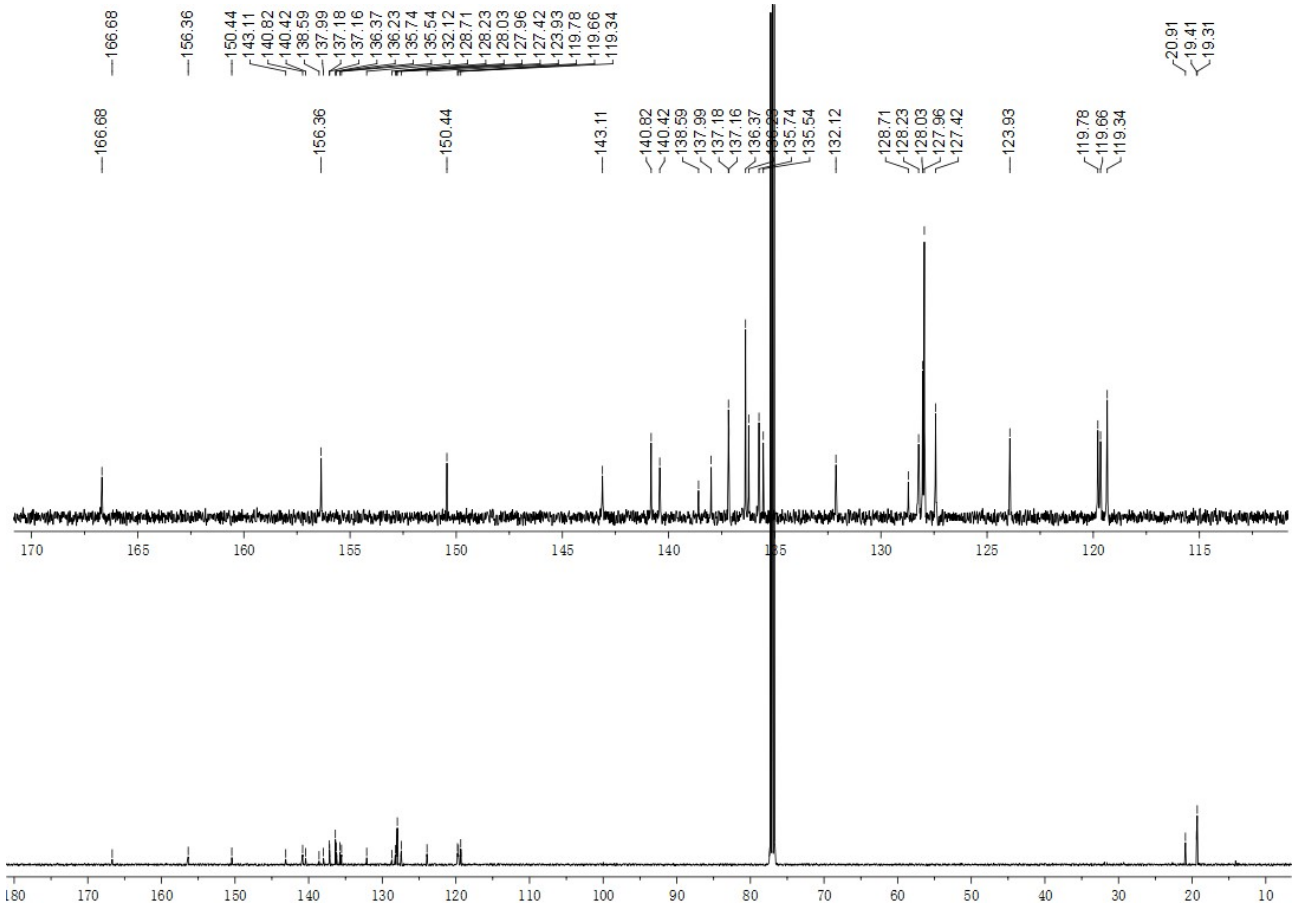

Figure S5.[13]C NMR spectrum of **3BF$_2$** in $CDCl_3$ at 298 K.

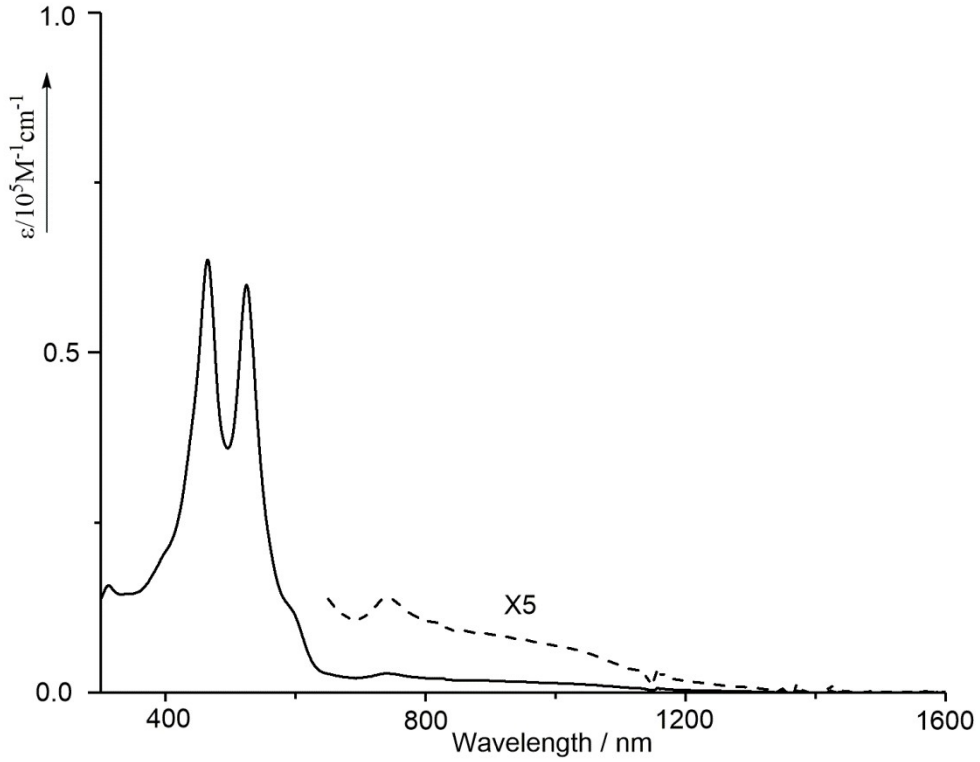

Figure S6. Absorption of **$3BF_2$** in CH_2Cl_2.

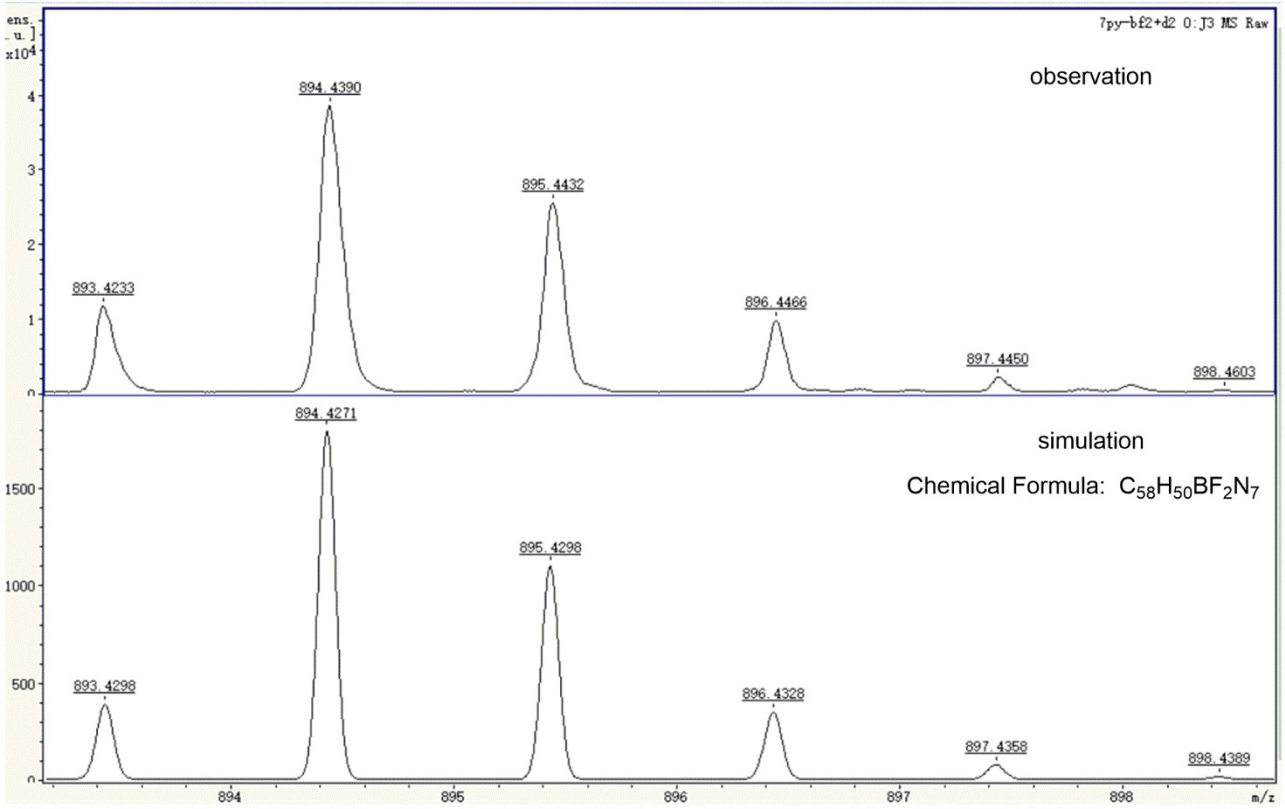

Figure S7. MALDI-TOF-MS spectra of **$3BF_2$**.

Synthesis of **3HCl**:

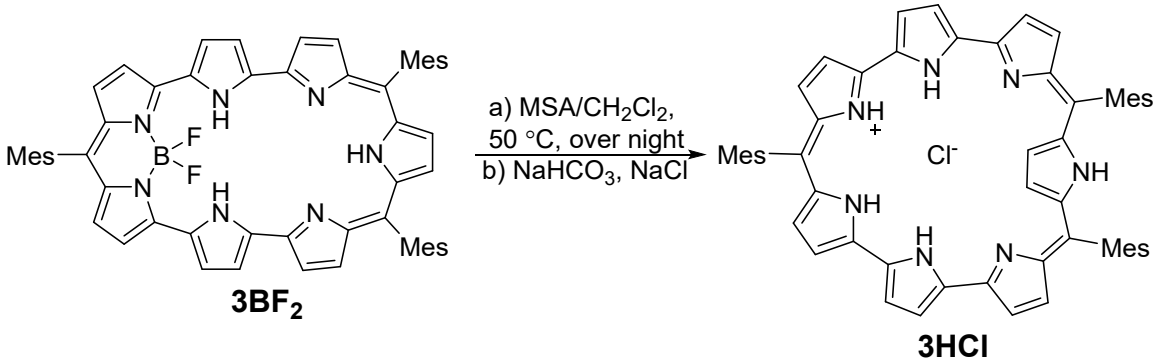

3BF$_2$ **3HCl**

Methanesulfonic acid (1.0 mL) was added to a solution of **3BF$_2$** (100 mg, 0.11 mmol) in dry CH_2Cl_2 (10 mL). The mixture was reflux for overnight. After cooling to room temperature, the mixture was first washed with aqueous $NaHCO_3$ and then brine once. The organic phase was dried over Na_2SO_4, and the solvent was removed under vacuum. The product was purified by recrystallization of MeOH/*n*-hexane to give **3HCl** (83.0 mg, 87% yield) as red solids.

3HCl: ^{1}H NMR (500 MHz, $CDCl_3$) δ = 25.42 (br, 1H, NH), 24.89 (br, 1H, NH), 16.79 (s, 1H, β-H), 6.50 (s, 2H, Ar-H), 6.49 (s, 2H, Ar-H), 6.43 (s, 4H, Ar-H), 6.36 (s, 2H, Ar-H), 4.76 (br, 1H, NH), 4.52 (br, 1H, β-H), 4.47 (br, 1H, β-H), 4.36 (br, 2H, β-H), 4.10 (d, J = 4.0 Hz, 2H, β-H), 4.03 (br, 2H, β-H), 4.01 (br, 2H, β-H), 3.86-3.84 (m, 3H, β-H), 3.73 (s, 1H, β-H), 3.72 (br, 1H, β-H), 3.55 (d, J = 4.0 Hz, 1H, β-H), 2.22 (s, 3H, Me-H), 2.18 (s, 3H, Me-H), 2.02 (m, 9H, Me-H), 1.95 (s, 6H, Me-H) and 1.89 (s, 6H, Me-H) ppm. Two NH protons and one outside β proton are not observed at room temperature. HR-MS (MALDI-TOF-MS): *m/z* = 846.4279, calcd for $(C_{58}H_{52}N_7)^+$ = 846.4279 ([M-Cl]$^+$). λ_{max} (ε [$M^{-1}cm^{-1}$]) = 396(36800), 491 (131000), 535 (200000) and 1088 (1700) nm.

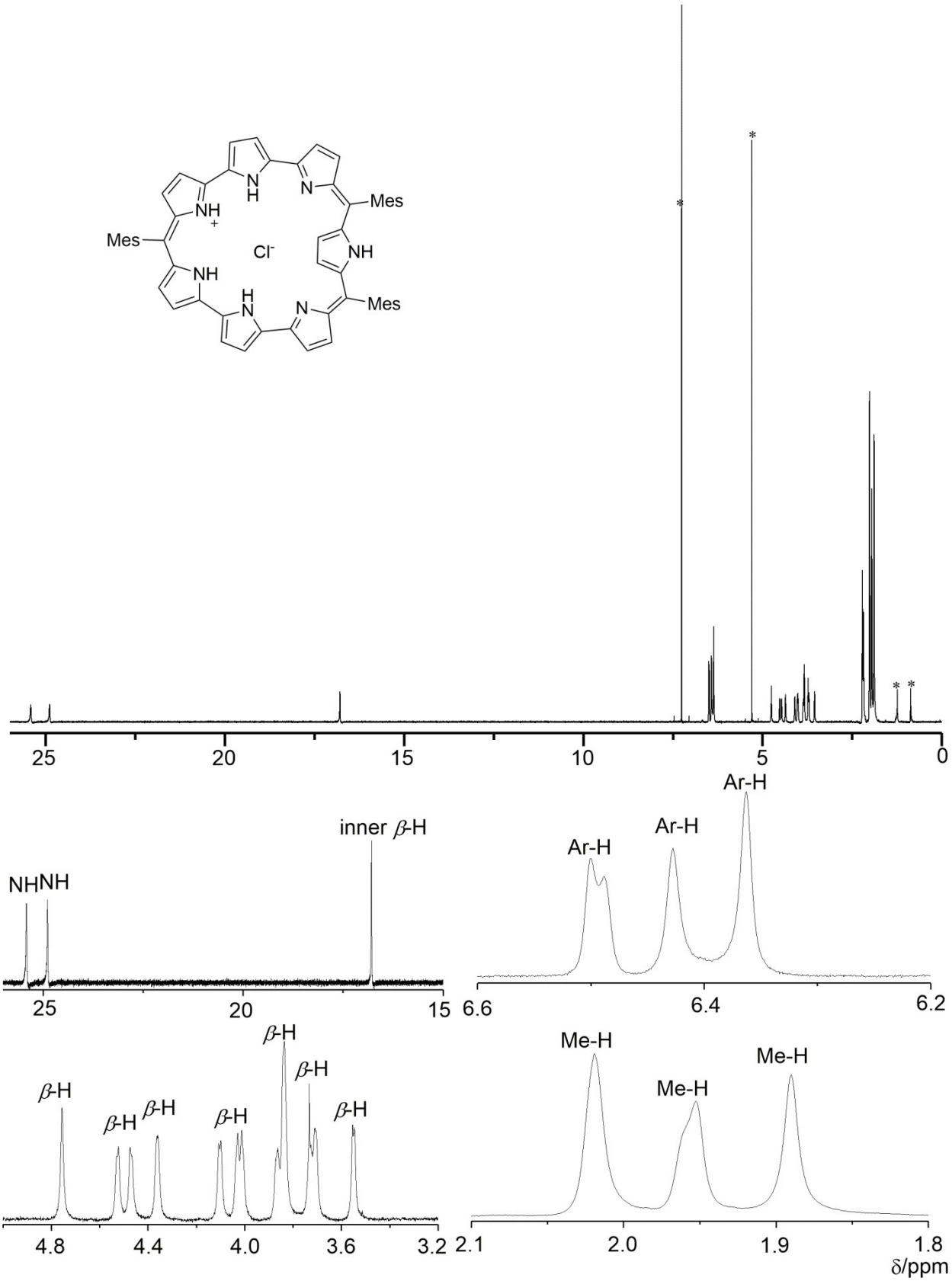

Figure S8. ^{1}H NMR spectrum of **3HCl** in $CDCl_3$ at 298 K. Asterisk means residual solvent or impurity.

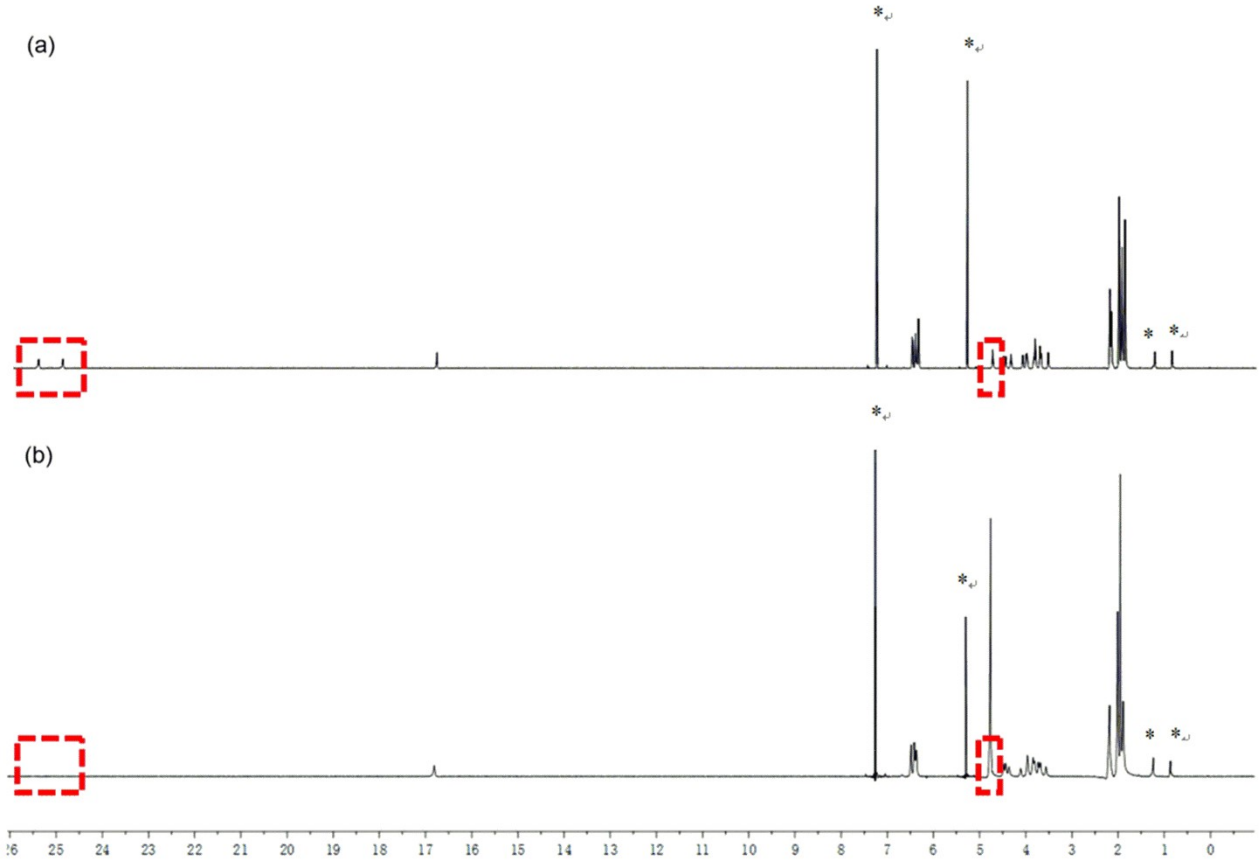

Figure S9. ^{1}H NMR spectra of **3HCl**; (a) at 298 K in $CDCl_3$ and (b) with D_2O. Asterisk means residual solvent or impurity.

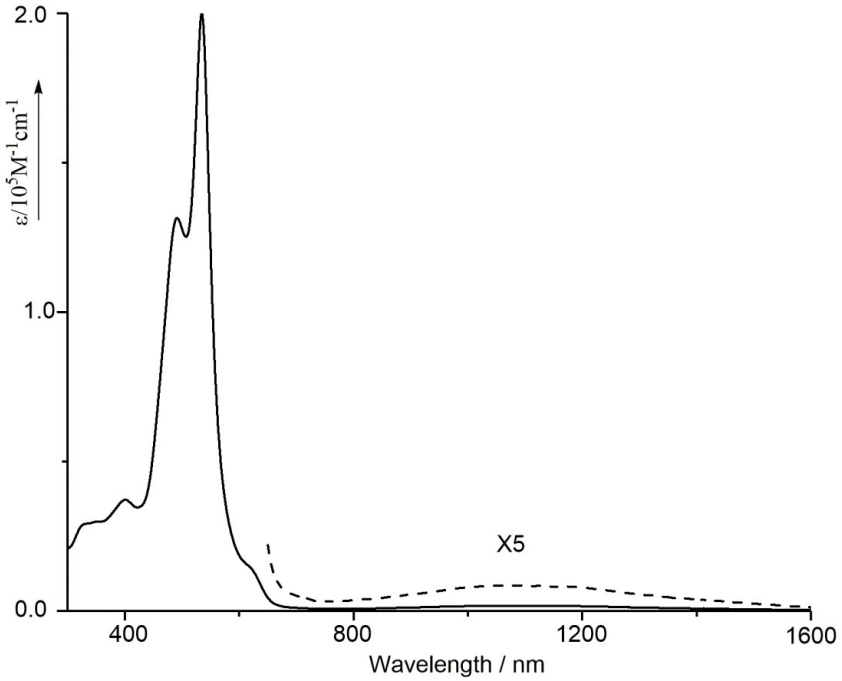

Figure S10. UV/Vis/NIR absorption spectrum of **3HCl** in CH_2Cl_2.

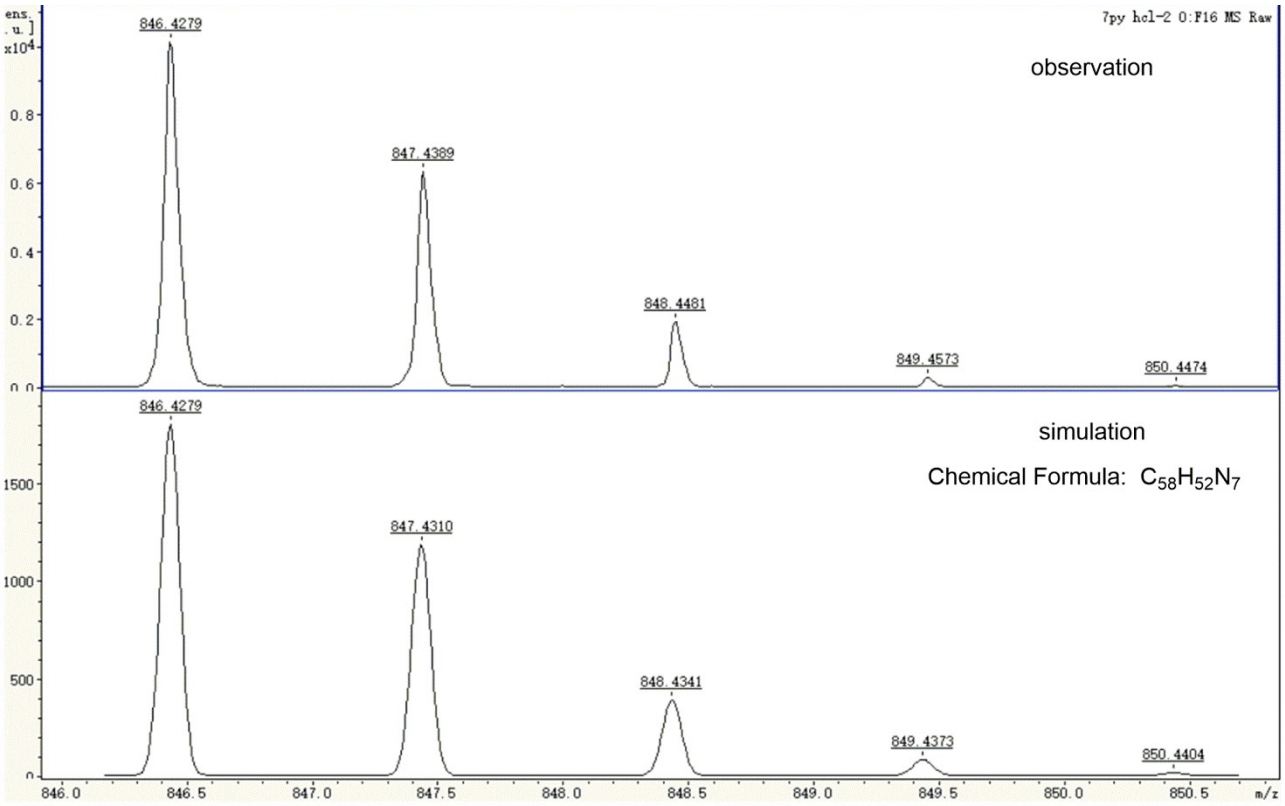

Figure S11.MALDI-TOF-MS spectra of **3HCl**.

Synthesis of **3**:

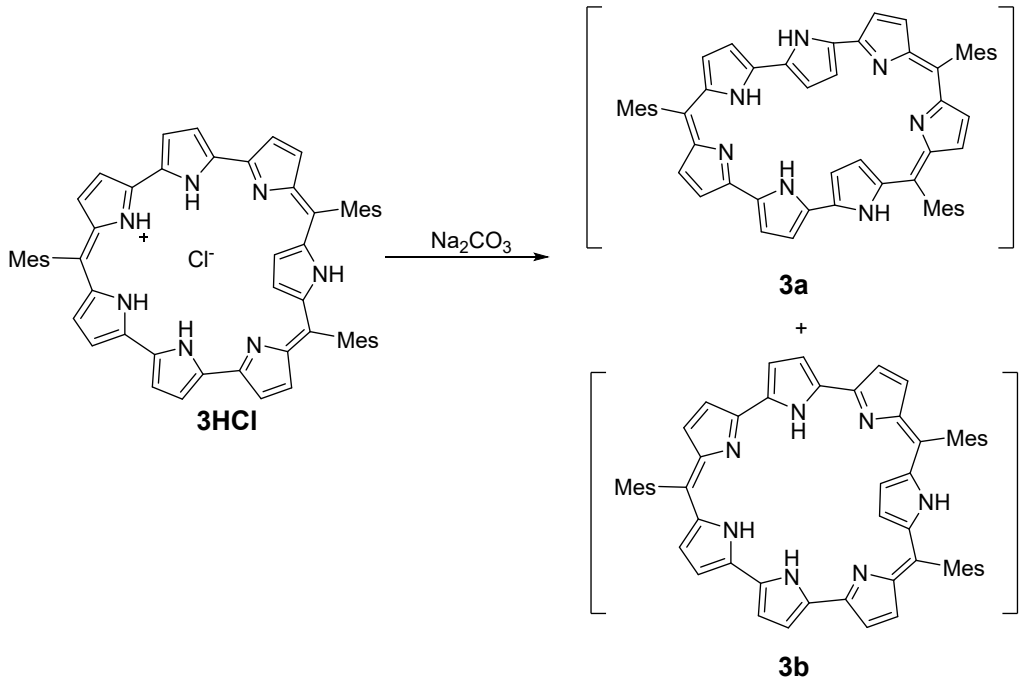

3HCl (30 mg, 0.034mmol) was dissolved in 20 mL CH_2Cl_2 and 30 mL saturated aqueous sodium carbonate

was added. The mixture was stirred vigorously for 10 min and the organic layer was separated and washed twice with water. Then organic phase was dried over Na_2SO_4, and the solvent was removed under vacuum. Precipitation with *n*-hexane/MeOH gave **3** (22.4 mg, 78% yield) as brown solids. Judging from the ^{1}H NMR spectrum, **3** was considered to consist of two isomers (**3a** and **3b**).

3a (Major isomer): ^{1}H NMR (500 MHz, DMSO-d6) δ = 19.25 (br, 1H, NH), 19.08 (br, 1H, NH), 10.97 (d, J = 4.4 Hz, 1H, β-H), 10.76 (d, J = 4.4 Hz, 1H, β-H), 10.11 (br, 1H, β-H), 9.95 (br, 1H, β-H), 6.89 (s, 4H, Ar-H), 6.85 (s, 2H, Ar-H), 6.08 (d, J = 4.4 Hz, 1H, β-H), 6.01 (d, J = 4.3 Hz, 1H, β-H), 5.95 (m, 2H, β-H), 5.89 (d, J = 4.4 Hz, 1H, β-H), 5.77 (d, J = 4.3 Hz, 1H, β-H), 5.52 (s, 1H, β-H), 5.32 (s, 1H, β-H), 5.21 (d, J = 3.6 Hz, 1H, β-H), 5.02 (d, J = 3.6 Hz, 1H, β-H), 2.23-2.22 (m, 9H, Me-H), 2.14-2.13 (m, 12H, Me-H) and 2.11 (br, 6H, Me-H) ppm; two NH are not observed at room temperature.

3b (Minor isomer): ^{1}H NMR (500 MHz, DMSO-d6) δ = 17.43 (br, 1H, inner NH), 15.46 (br, 2H, inner NH), 10.91 (s, 2H, β-H), 7.05 (br, 1H, outer NH), 6.78 (s, 2H, Ar-H), 6.74 (s, 4H, Ar-H), 5.87 (d, J = 4.7 Hz, 2H, β-H), 5.60 (d, J = 2.7 Hz, 2H, β-H), 5.52 – 5.48 (m, 4H, β-H), 5.47 (d, J = 4.3 Hz, 2H, β-H), 4.95 (d, J = 2.7 Hz, 2H, β-H), 2.24 (s, 3H, Me-H), 2.17 (s, 6H, Me-H), 2.08 (s, 6H, Me-H) and 1.96 (s, 12H, Me-H) ppm.

HR-MS (MALDI-TOF-MS): m/z = 846.4279, calcd for $(C_{58}H_{52}N_7)^+$ = 846.4298 ($[M+H]^+$); λ_{max} (ε [$M^{-1}cm^{-1}$]) = 338 (21600), 483 (72100), 801 (1300) nm.

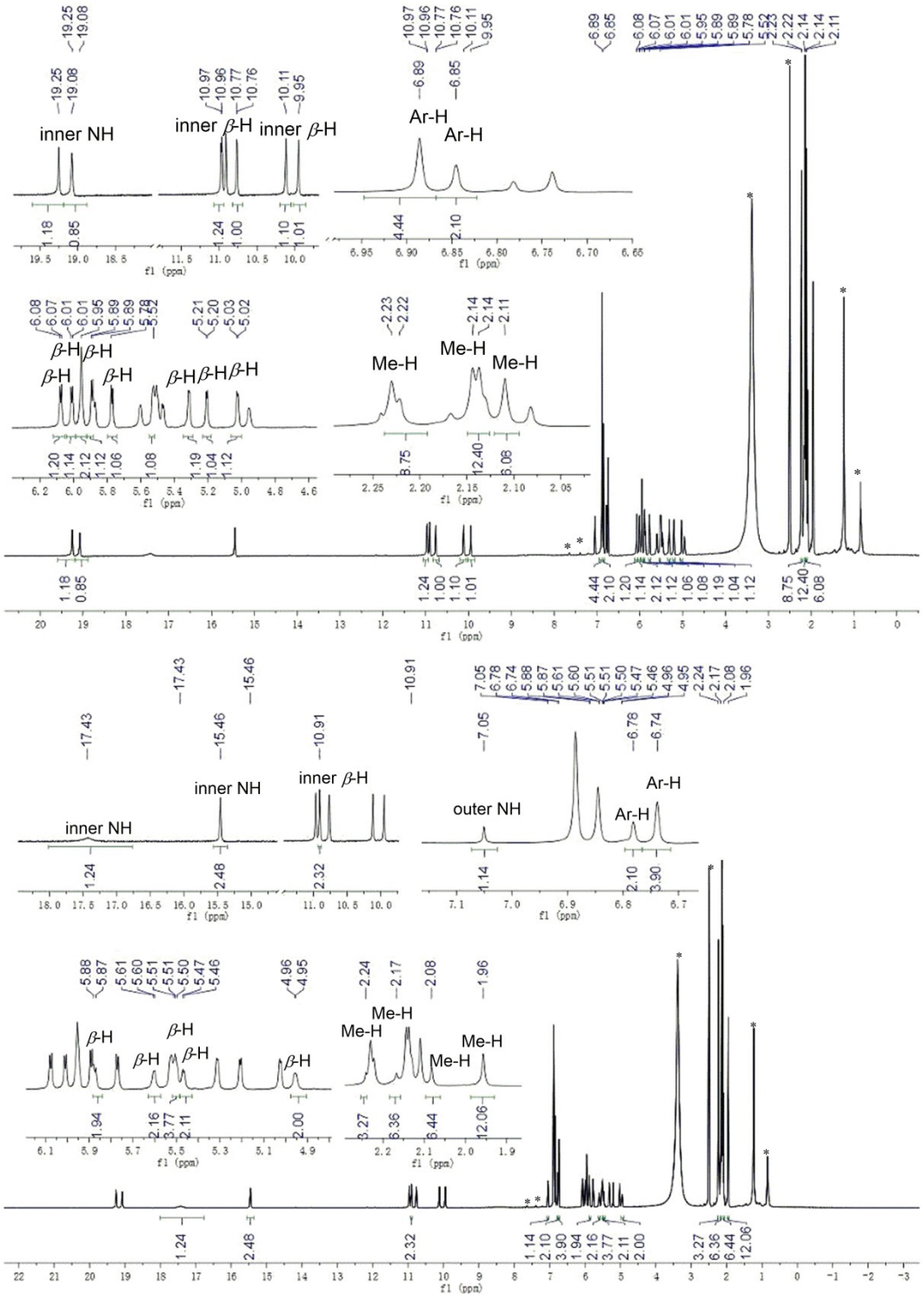

Figure S12 ^{1}H NMR spectrum of **3** in DMSO-d_8 at 298 K; upper: assignments for **3a** (Major isomer), bottom: assignments for **3b** (Minor isomer). Asterisk means residual solvent or impurity.

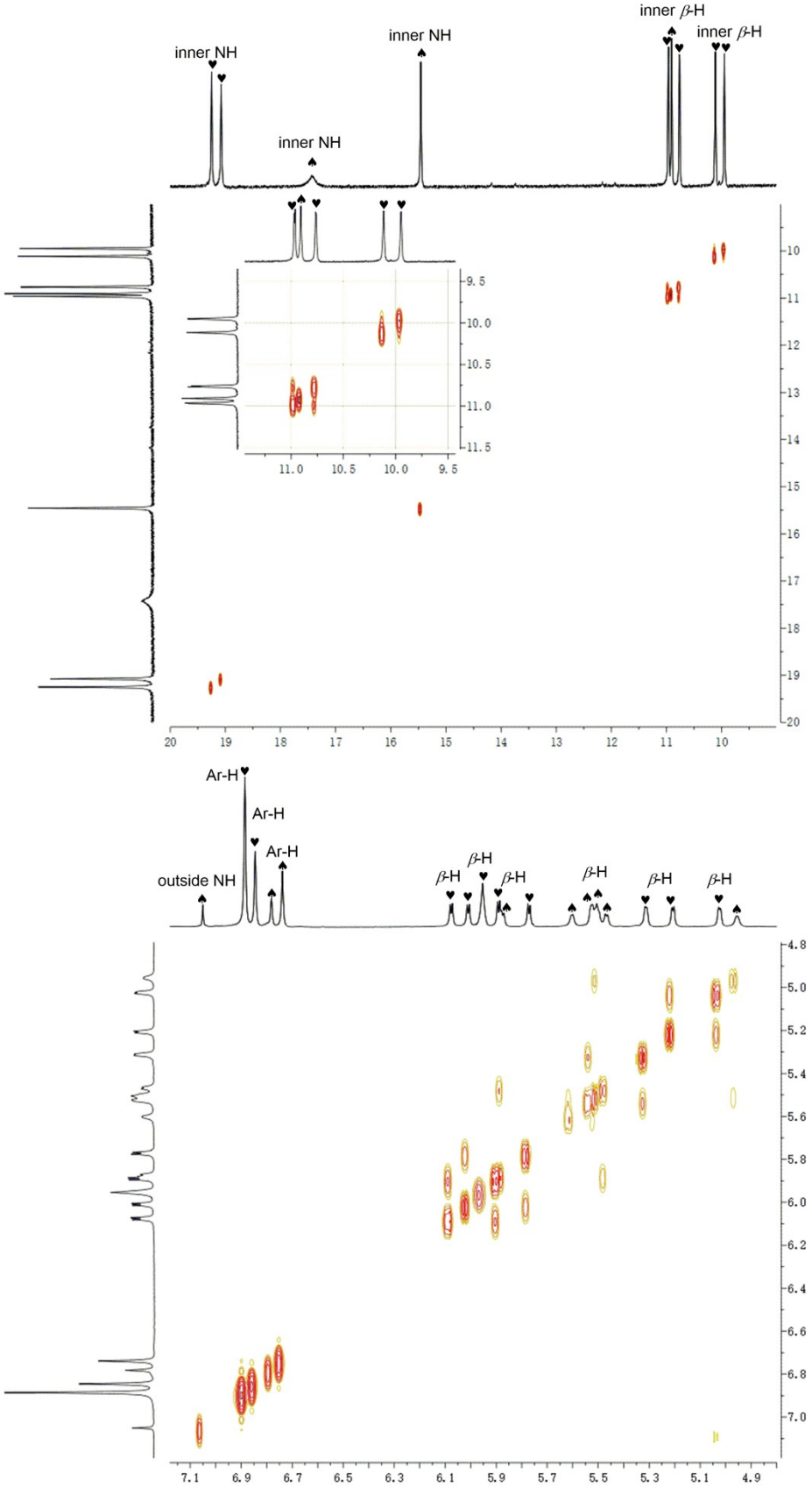

Figure S13 ^{1}H-^{1}H COSY of **3** in DMSO-d_8 at 298 K; peaks due to **3a** (♥) or **3b** (♠).

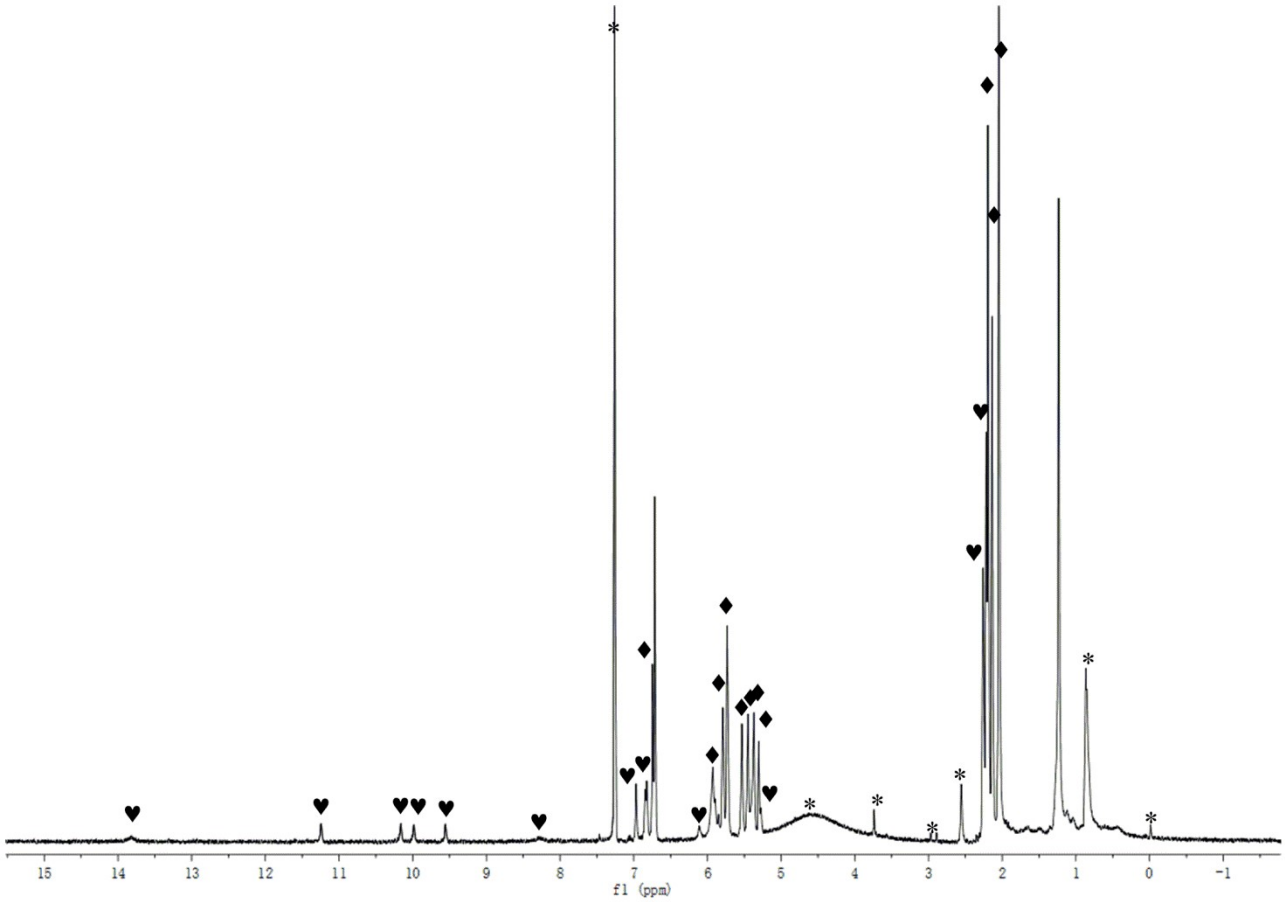

Figure S14.[1]H NMR spectrum of **3** in $CDCl_3$ at 273 K; peaks due to **3a** (♥) or **3b** (♦). Asterisk means residual solvent or impurity.

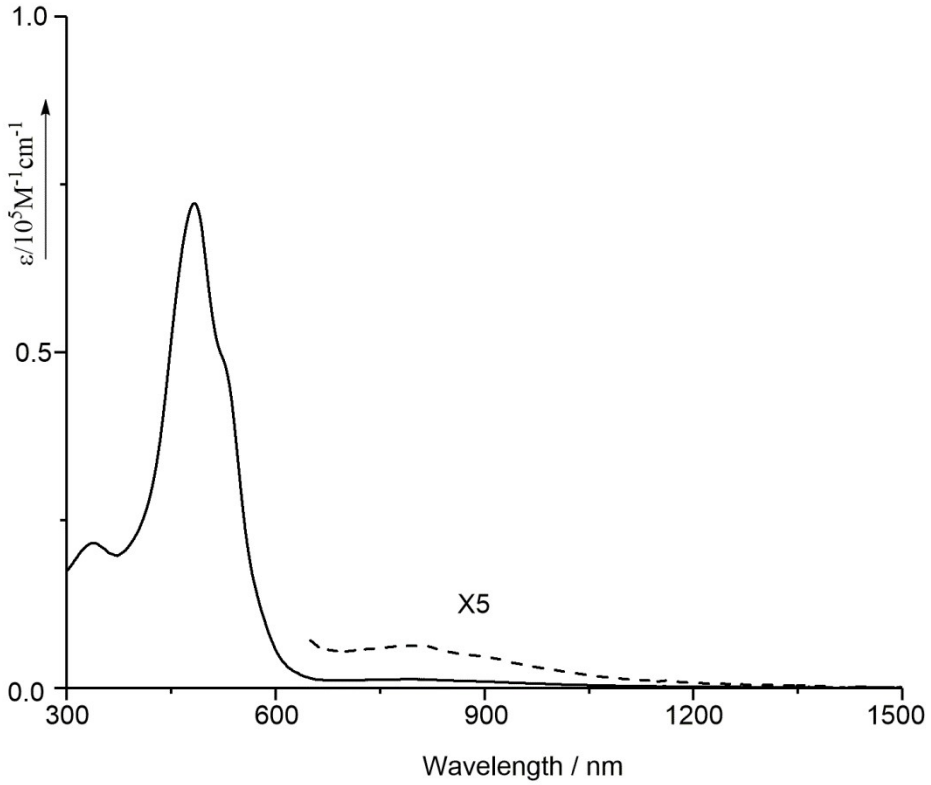

Figure S15. UV/Vis/NIR absorption spectrum of **3** in CH_2Cl_2.

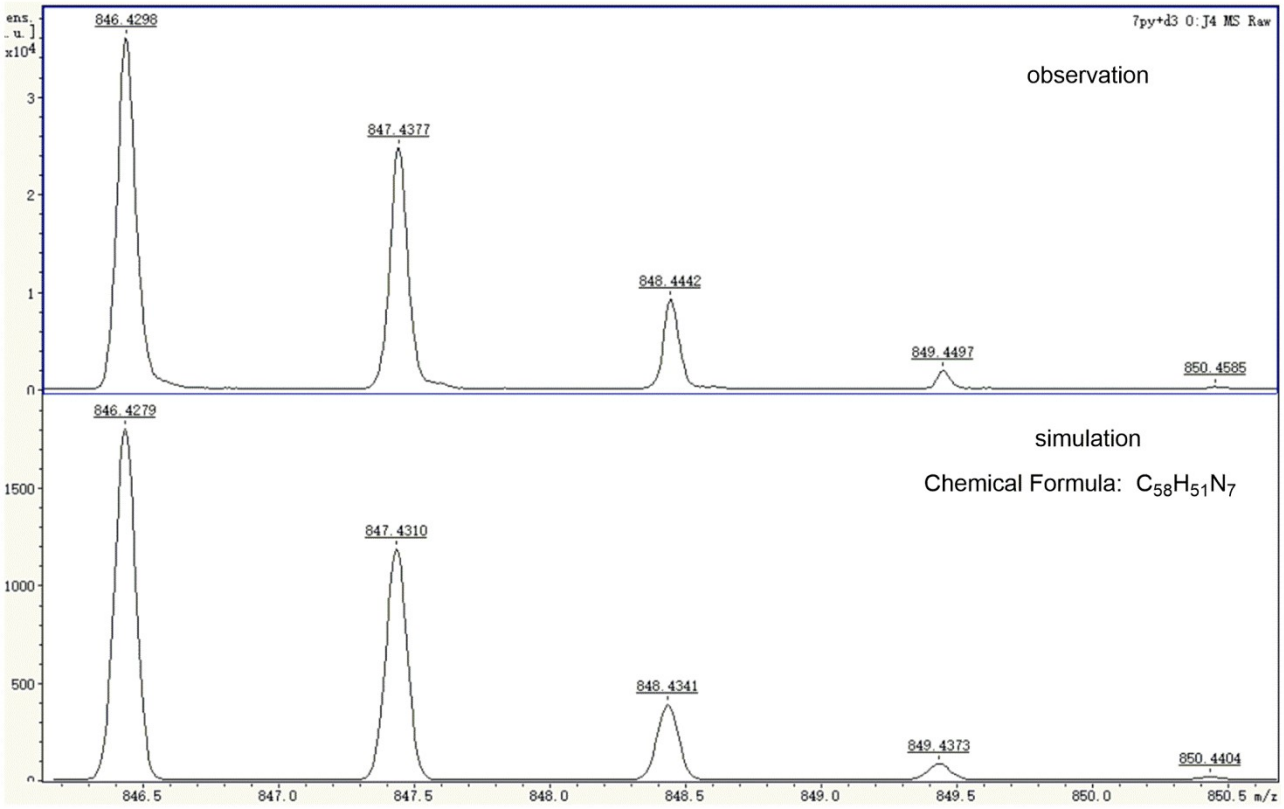

Figure S16. MALDI-TOF-MS spectra of **3**.

Synthesis of **3Pd$_2$**:

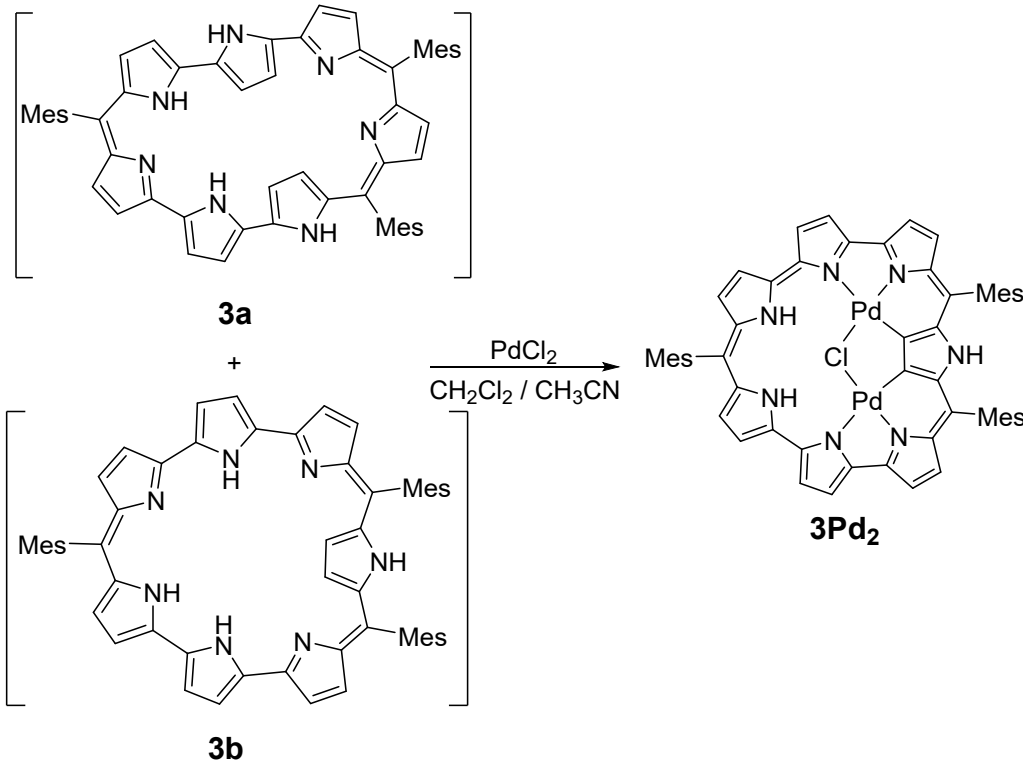

To a solution of **3** (50.0 mg, 0.059 mmol) in a mixture of CH_2Cl_2/CH_3CN (50/10 mL) was added $PdCl_2$ (104.6 mg, 0.59 mmol, 10.0 equiv.). After stirring for 4 h, insoluble materials was removed by flash Al_2O_3 chromatography (CH_2Cl_2 as an eluent). The solvent was removed under vacuum and residue was separated by Al_2O_3 column chromatography (CH_2Cl_2/*n*-hexane as an eluent). Recrystallization with CH_2Cl_2/*n*-hexane gave **3Pd$_2$** (12.3 mg, 19 % yield) as blue solids.

3Pd$_2$: ^{1}H NMR (500 MHz, $CDCl_3$) δ = 42.93 (br, 2H, inner-NH), 5.49 (s, 2H, Ar-H), 5.21 (s, 4H, Ar-H), 2.28 (s, 9H, Me-H), 2.04 (s, 18H, Me-H), -1.06 (br, 2H, β-H), -1.35 (br, 2H, β-H), -1.43 (br, 2H, β-H), -1.74 (br, 2H, β-H), -1.86 (br, 2H, β-H), -1.90 (br, 2H, β-H) and -6.17 (br, 1H, outer-NH) ppm. HR-MS (MALDI-TOF-MS): *m/z* = 1091.1711, calcd for $(C_{58}H_{48}ClN_7Pd_2)^+$ = 1091.1745 ($[M+H]^+$). λ_{max} (ε [$M^{-1}cm^{-1}$]) = 398(31300), 438(30800), 473(29300), 606(136000) and 941(6000) nm.

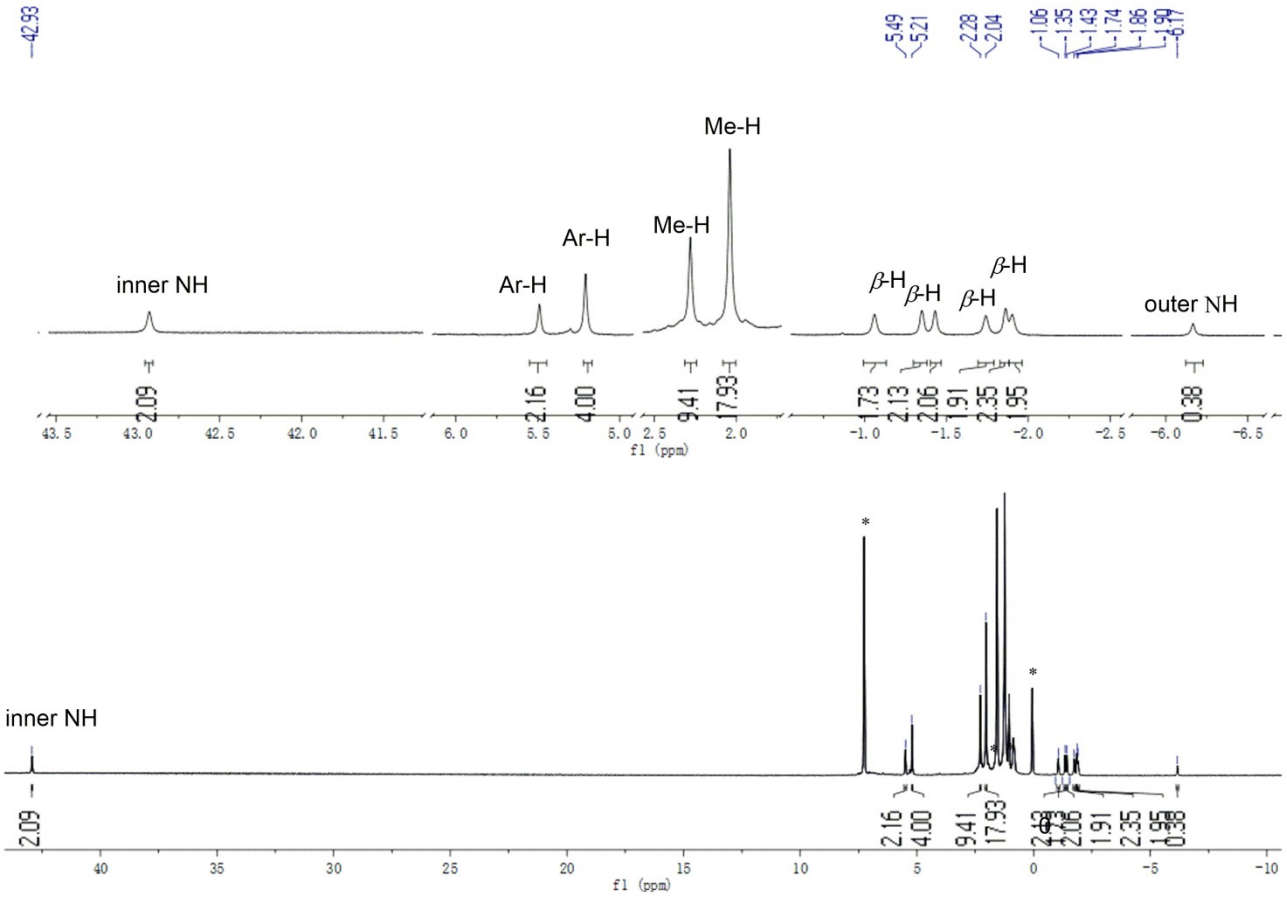

Figure S17. ^{1}H NMR spectrum of **3Pd$_2$** in $CDCl_3$ at 298K. Asterisk means residual solvent or impurity.

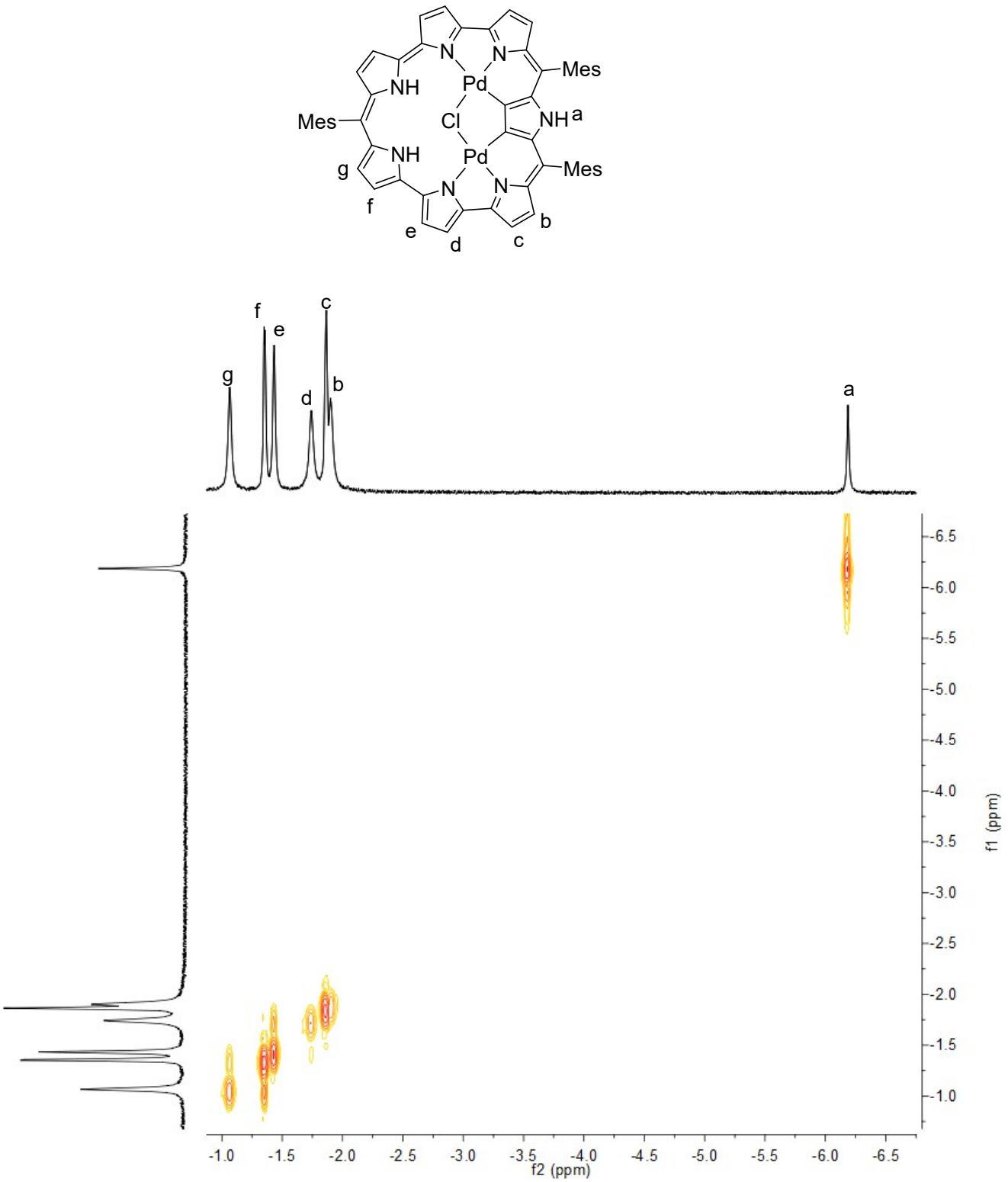

Figure S18. ^{1}H-^{1}H COSY spectrum of **3Pd$_2$** in $CDCl_3$ at 298K.

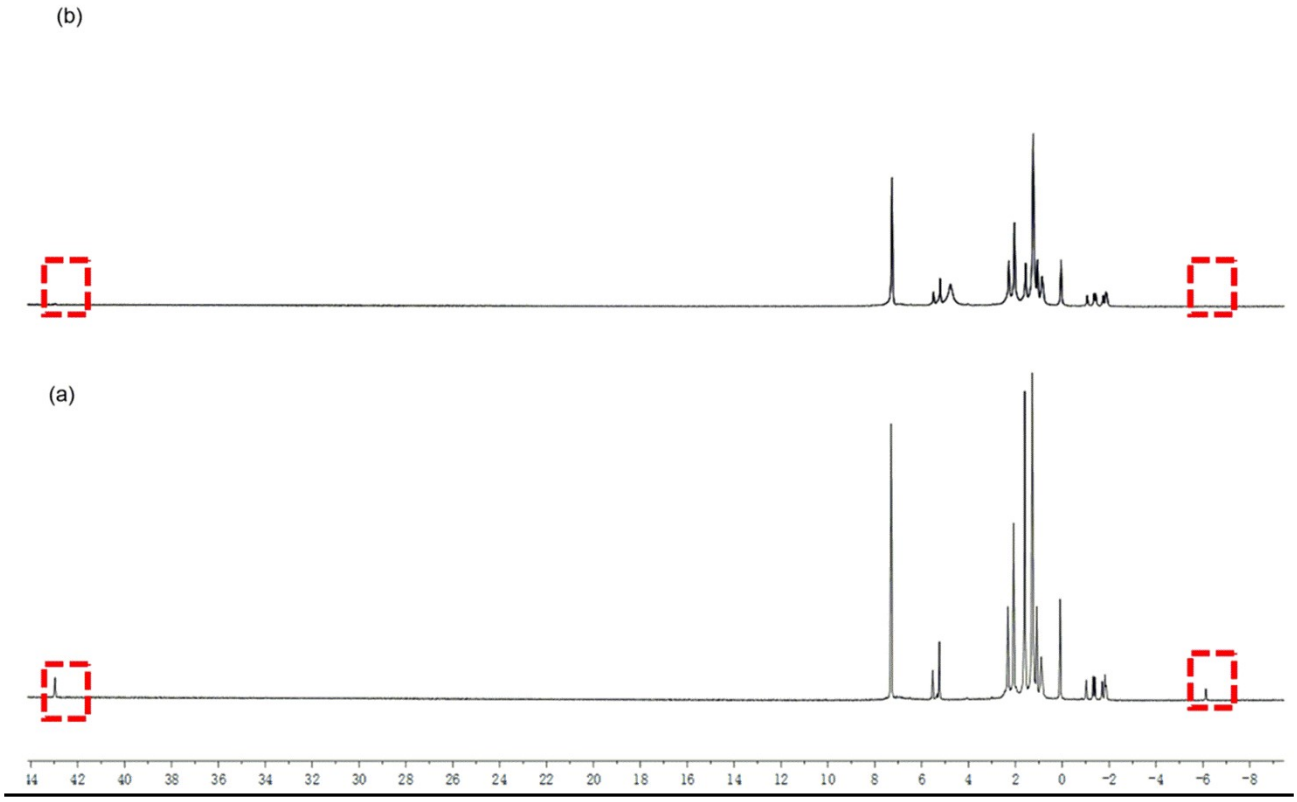

Figure S19. ^{1}H NMR spectra of **3Pd$_2$**; (a) at 298 K in $CDCl_3$ and (b) with D_2O.

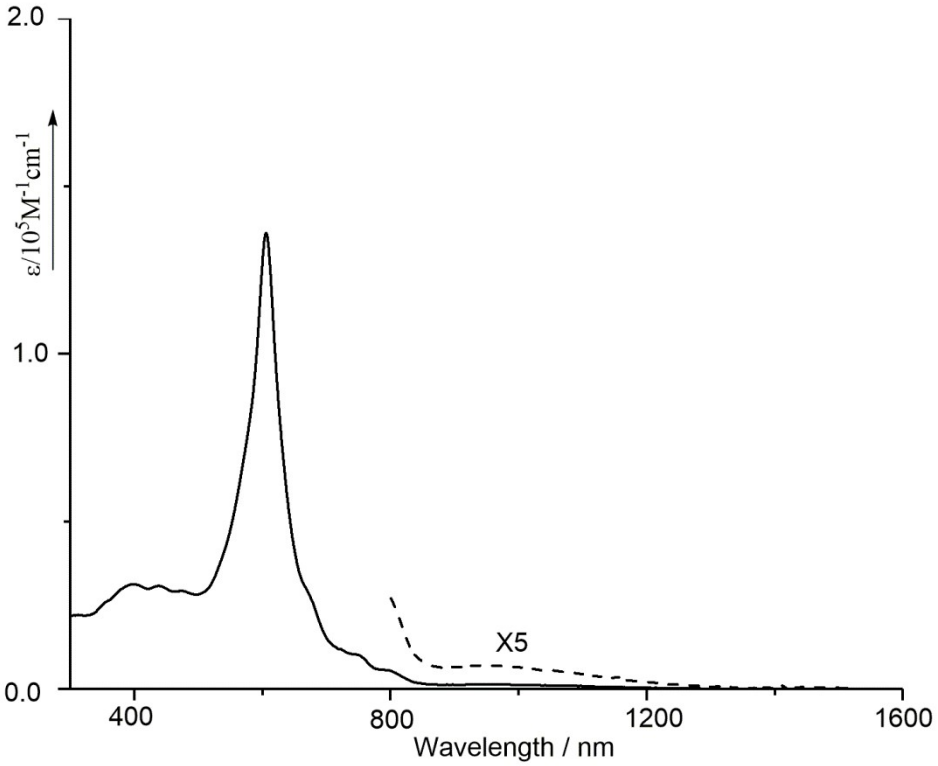

Figure S20. UV/Vis/NIR absorption spectrum of **3Pd$_2$** in CH_2Cl_2.

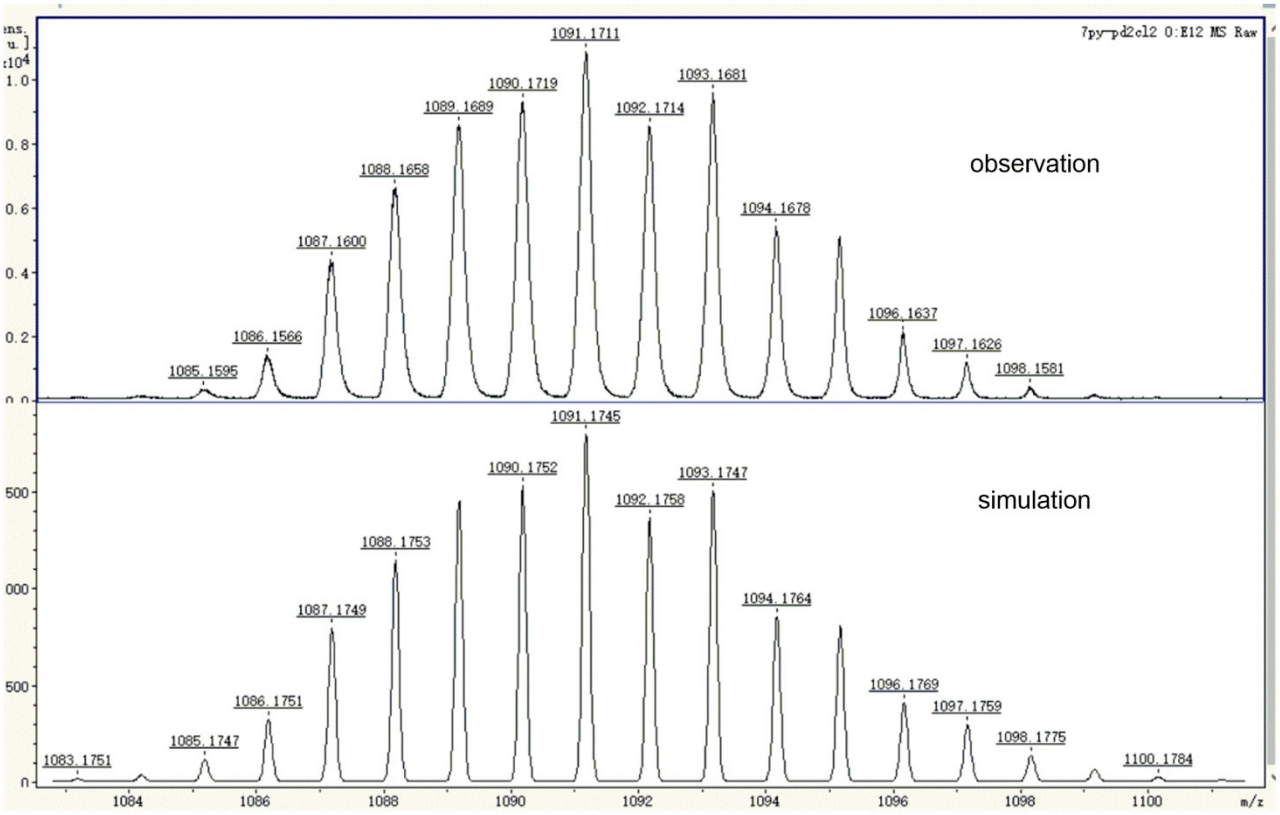

Figure S21. MALDI-TOF-MS spectra of **3Pd$_2$**; (a) observed and (b) calculated.

X-Ray Crystal Data

Table S1. Crystal data and structure refinement for **$3BF_2$**.

Empirical formula	$C_{116}\,H_{100}\,B_2\,F_4\,N_{14}$	
Formula weight	1787.71	
Temperature	100.0(9) K	
Wavelength	1.54184 Å	
Crystal system	Monoclinic	
Space group	P 1 21 1	
Unit cell dimensions	a = 11.9268(3) Å	α= 90°.
	b = 27.7816(9) Å	β= 105.272(3)°.
	c = 16.3663(5) Å	γ = 90°.
Volume	5231.4(3) $Å^3$	
Z	2	
Density (calculated)	1.135 Mg/m^3	
Absorption coefficient	0.573 mm^{-1}	
F(000)	1880	
Crystal size	0.1 x 0.1 x 0.05 mm^3	
Theta range for data collection	2.799 to 66.601°.	
Index ranges	-11<=h<=14, -33<=k<=32, -19<=l<=18	
Reflections collected	19567	
Independent reflections	13478 [R(int) = 0.0479]	
Completeness to theta = 66.601°	99.9 %	
Absorption correction	Semi-empirical from equivalents	
Max. and min. transmission	1.00000 and 0.83273	
Refinement method	Full-matrix least-squares on F^2	
Data / restraints / parameters	13478 / 1 / 1243	
Goodness-of-fit on F^2	1.023	
Final R indices [I>2sigma(I)]	R1 = 0.0656, wR2 = 0.1563	
R indices (all data)	R1 = 0.0894, wR2 = 0.1724	
Absolute structure parameter	0.9(2)	
Extinction coefficient	n/a	
Largest diff. peak and hole	0.531 and -0.275 $e.Å^{-3}$	
CCDC number	2330167	

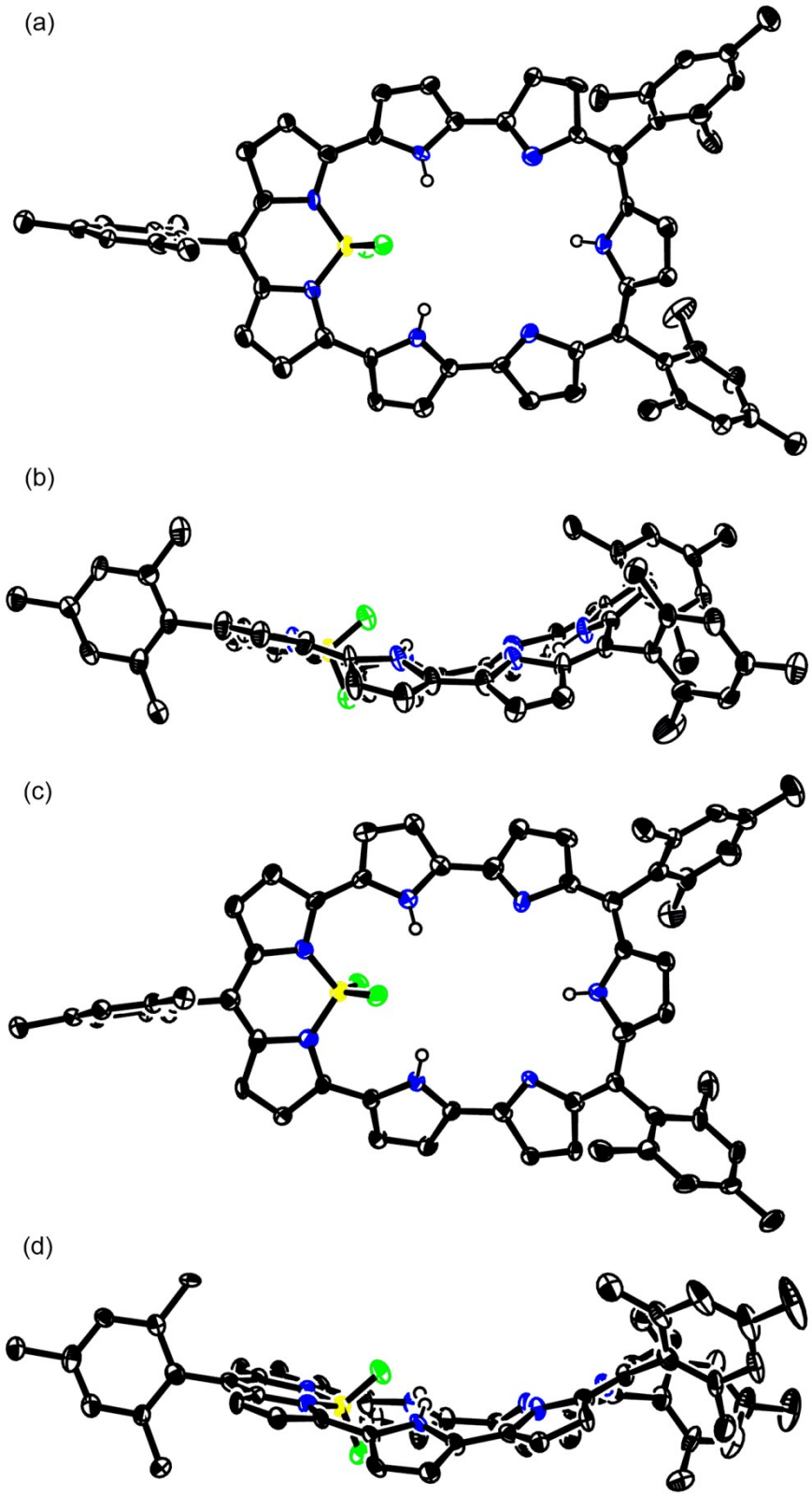

Figure S22. X-ray crystal structure of **3BF$_2$**; (a) top view and (b) side view of **3BF$_2$A,** and (c) top view and (d) side view of **3BF$_2$B**. The thermal ellipsoids are 50% probability level. Peripheral protons are omitted for clarity

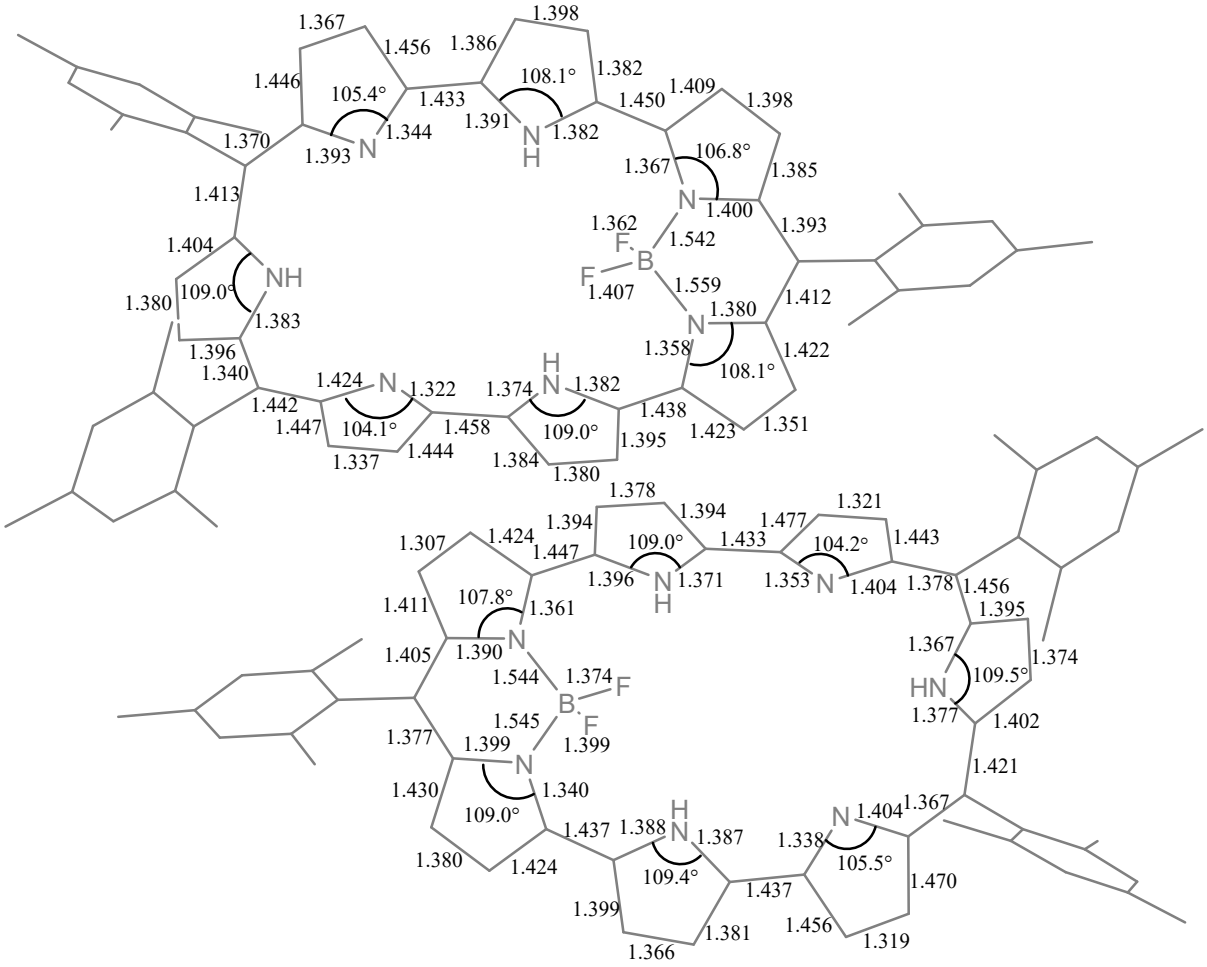

Figure S23. Bond lengths and bond angles of **3BF$_2$A** and **3BF$_2$B**.

Table S2. Crystal data and structure refinement for **3HCl**.

Empirical formula	$C_{63}\ H_{59}\ Cl_4\ N_9$	
Formula weight	882.55	
Temperature	99.9(5) K	
Wavelength	1.54184 Å	
Crystal system	Monoclinic	
Space group	P 1 21/c 1	
Unit cell dimensions	a = 10.7069(7) Å	α= 90°.
	b = 16.7483(6) Å	β= 91.717(4) °.
	c = 31.0611(12) Å	γ = 90°.
Volume	5567.4(5) $Å^3$	
Z	4	
Density (calculated)	1.293 Mg/m^3	
Absorption coefficient	2.315 mm^{-1}	
F(000)	2272	
Crystal size	0.2 x 0.2 x 0.1 mm^3	
Theta range for data collection	2.847 to 66.593°.	
Index ranges	-12<=h<=11, -19<=k<=12, -34<=l<=36	
Reflections collected	20151	
Independent reflections	9836 [R(int) = 0.0505]	
Completeness to theta = 66.593°	100.0 %	
Absorption correction	Semi-empirical from equivalents	
Max. and min. transmission	1.00000 and 0.41247	
Refinement method	Full-matrix least-squares on F^2	
Data / restraints / parameters	9836 / 0 / 723	
Goodness-of-fit on F^2	1.063	
Final R indices [I>2sigma(I)]	R1 = 0.0729, wR2 = 0.1843	
R indices (all data)	R1 = 0.0916, wR2 = 0.1975	
Extinction coefficient	n/a	
Largest diff. peak and hole	0.729 and -1.279 $e.Å^{-3}$	
CCDC number	2330168	

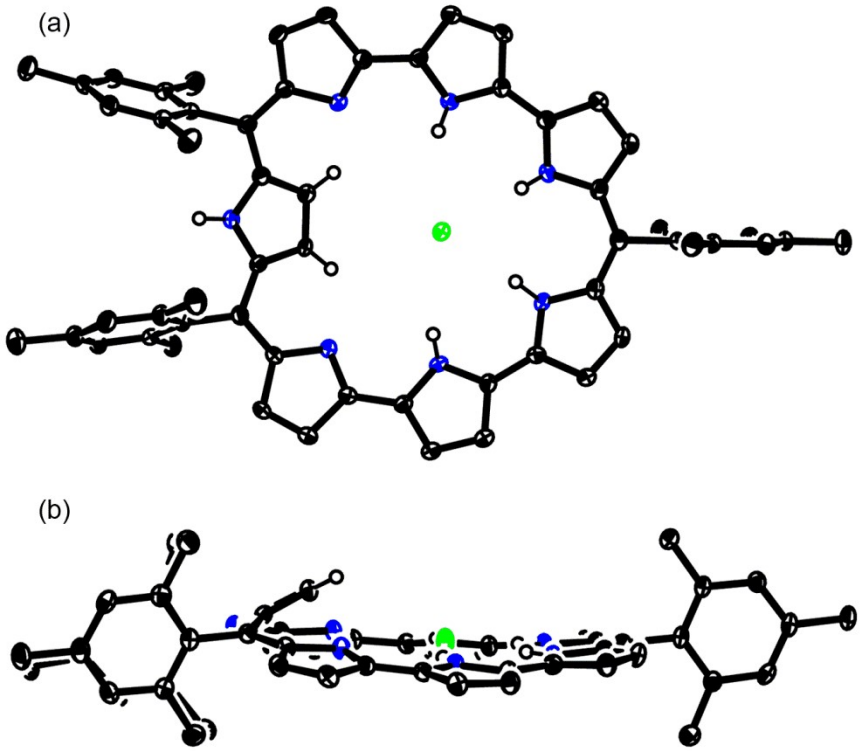

Figure S24. X-ray crystal structure of **3HCl**. The thermal ellipsoids are 50% probability level. Peripheral β-protons and solvent molecules are omitted for clarity.

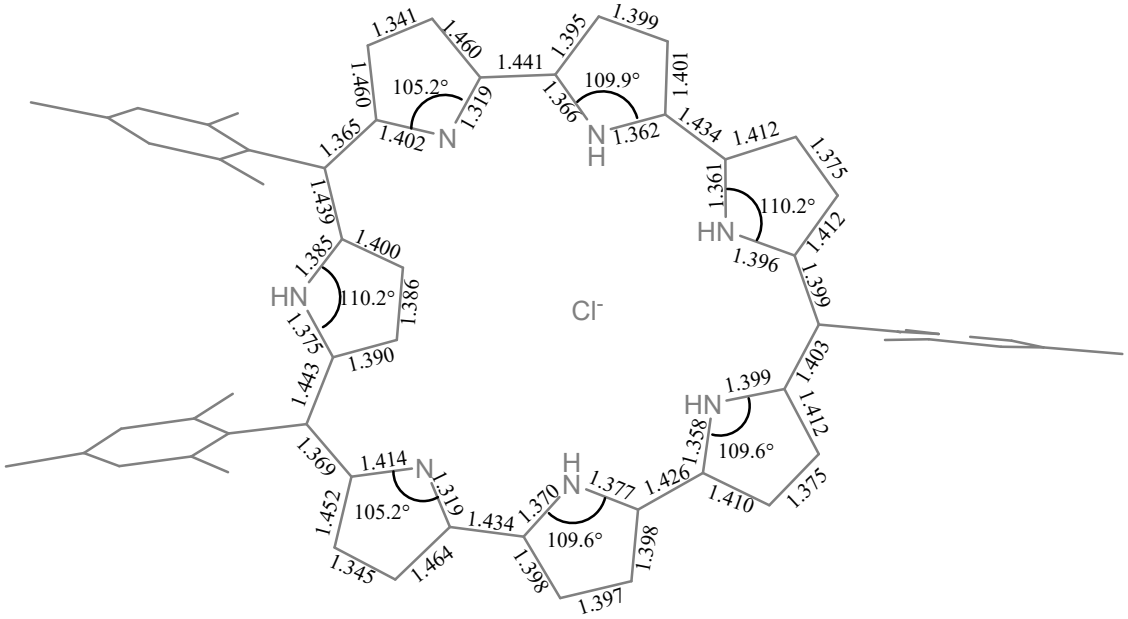

Figure S25. Bond lengths and bond angles of **3HCl**.

Table S3. Crystal data and structure refinement for **$3Pd_2$**.

Empirical formula	C_{58} H_{48} Cl N_7 Pd_2	
Formula weight	1091.28	
Temperature	100.01(10) K	
Wavelength	1.54184 Å	
Crystal system	Orthorhombic	
Space group	Pnma	
Unit cell dimensions	a = 14.5782(3) Å	α= 90°.
	b = 19.0441(4) Å	β= 90°.
	c = 16.8698(5) Å	γ = 90°.
Volume	4683.5(2) $Å^3$	
Z	4	
Density (calculated)	1.548 Mg/m^3	
Absorption coefficient	7.097 mm^{-1}	
F(000)	2216	
Crystal size	0.1 x 0.1 x 0.05 mm^3	
Theta range for data collection	3.500 to 66.597°.	
Index ranges	-17<=h<=17, -22<=k<=22, -20<=l<=19	
Reflections collected	59585	
Independent reflections	4276 [R(int) = 0.0588]	
Completeness to theta = 66.597°	100.0 %	
Absorption correction	Semi-empirical from equivalents	
Max. and min. transmission	1.00000 and 0.07529	
Refinement method	Full-matrix least-squares on F^2	
Data / restraints / parameters	4276 / 0 / 329	
Goodness-of-fit on F^2	1.102	
Final R indices [I>2sigma(I)]	R1 = 0.0549, wR2 = 0.1348	
R indices (all data)	R1 = 0.0592, wR2 = 0.1376	
Extinction coefficient	n/a	
Largest diff. peak and hole	1.512 and -1.080 $e.Å^{-3}$	
CCDC number	2330169	

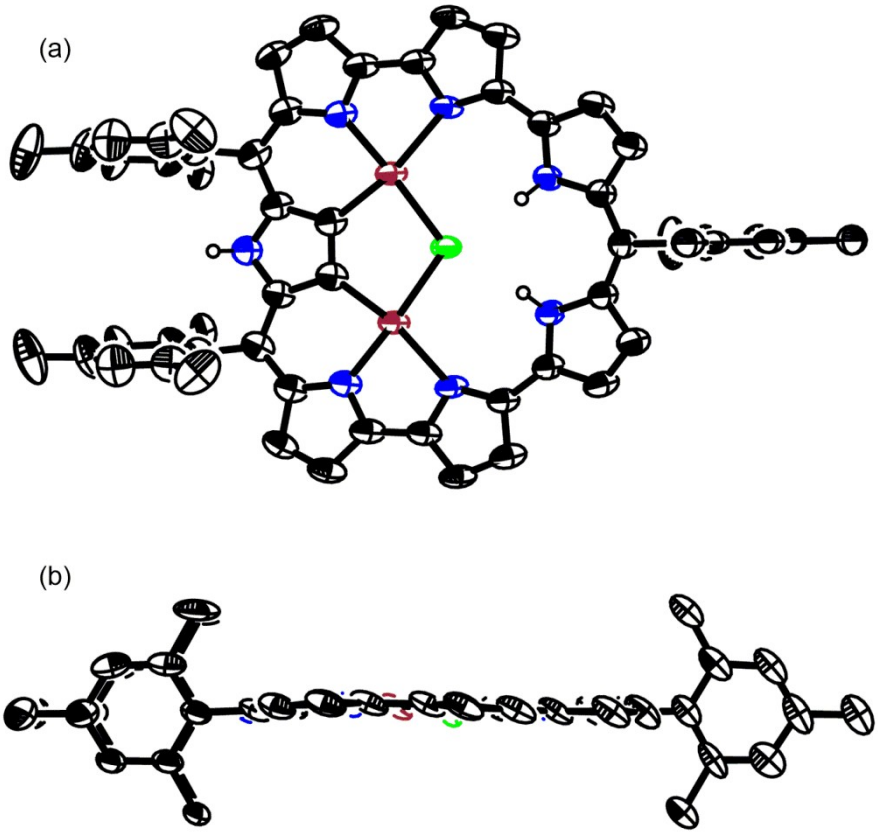

Figure S26. X-ray crystal structure of **3Pd$_2$**. The thermal ellipsoids are 50% probability level. Peripheral β-protons and solvent molecules are omitted for clarity.

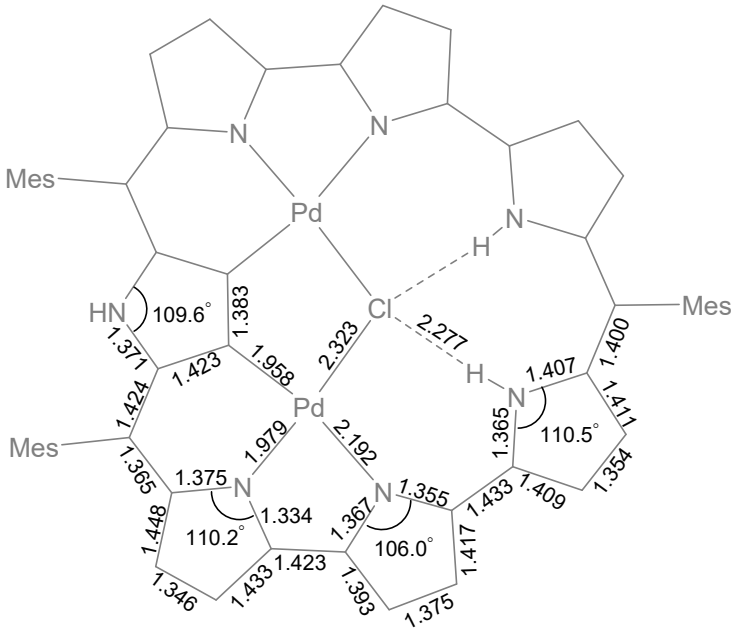

Figure S27. Structural analysis of **3Pd$_2$**.

Electrochemical Data

Table S4. CV and DPV of **$3BF_2$**, **3HCl**, **3** and **$3Pd_2$** in CH_2Cl_2 with 0.1 M Bu_4NPF_6. Potentials were determined vs ferrocene/ferrocenium ion by differential pulse voltammograms. Working electrode: glassy carbon. Counter electrode: Pt wire. Reference electrode: Ag/Ag^+. Scan rate: 30 mV/s

Sample	$E_{red.3}$ (V)	$E_{red.2}$ (V)	$E_{red.1}$ (V)	$E_{ox.1}$ (V)	$E_{ox.2}$ (V)	$E_{ox.3}$ (V)	ΔE_{HL}[b]
$3BF_2$	-	-1.37	-1.15	0.10	0.42	-	1.25
3HCl	-1.57	-1.23	-0.78	-0.04	0.39	-	0.74
3	-1.76	-1.45	-1.16	-0.14	0.15	0.34	1.30
$3Pd_2$	-1.79	-1.33	-0.95	-0.23	0.25	-	0.72

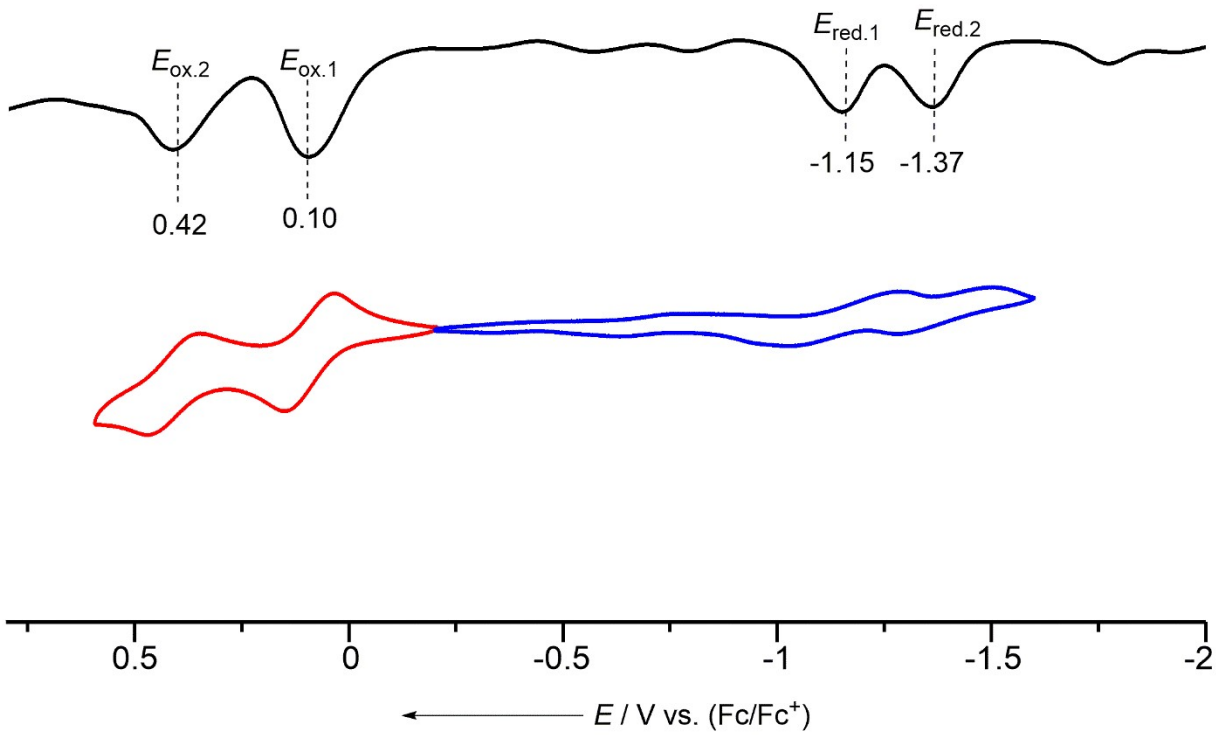

Figure S28. Cyclic voltammogram and differential pulse voltammogram of **$3BF_2$**.

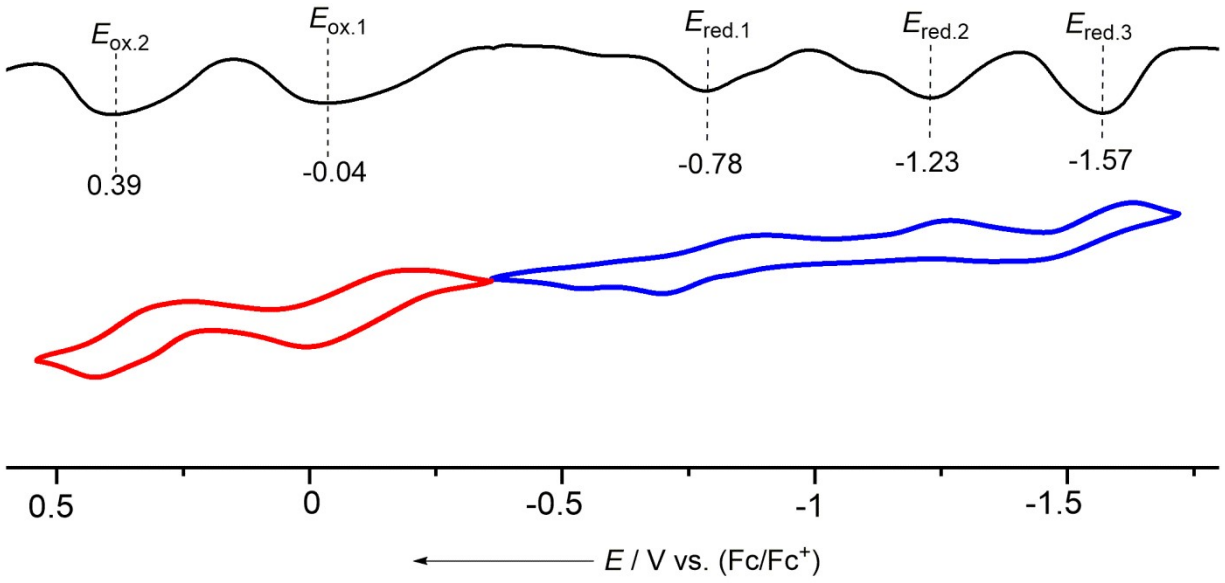

Figure S29. Cyclic voltammogram and differential pulse voltammogram of **3HCl**.

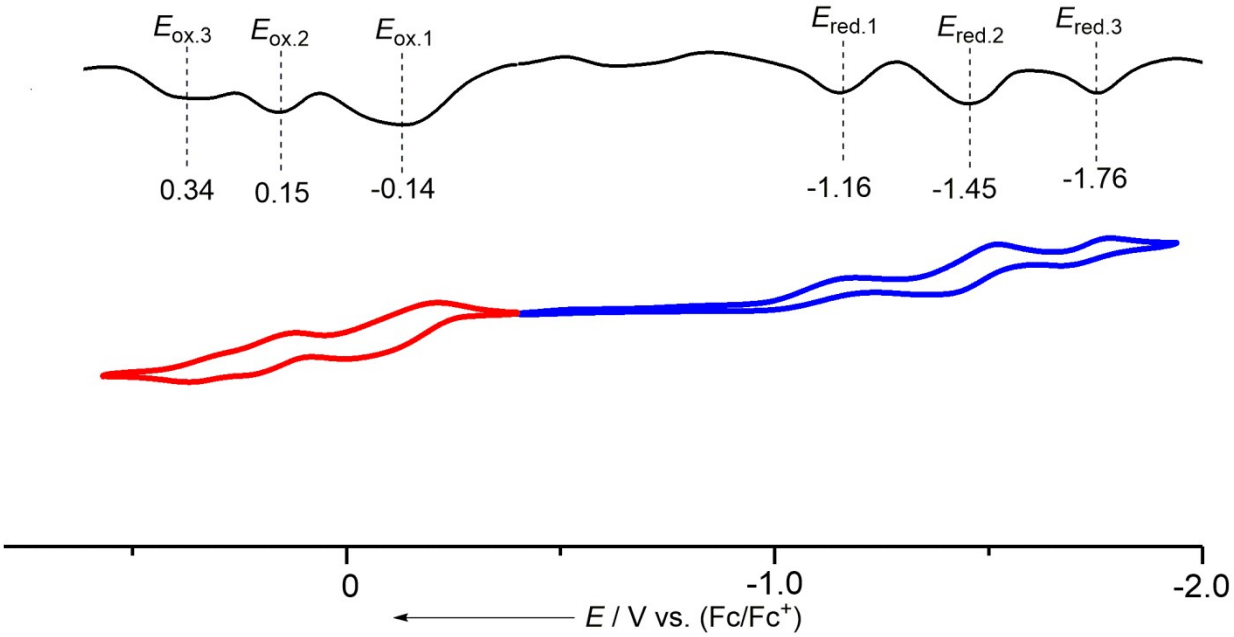

Figure S30. Cyclic voltammogram and differential pulse voltammogram of **3**.

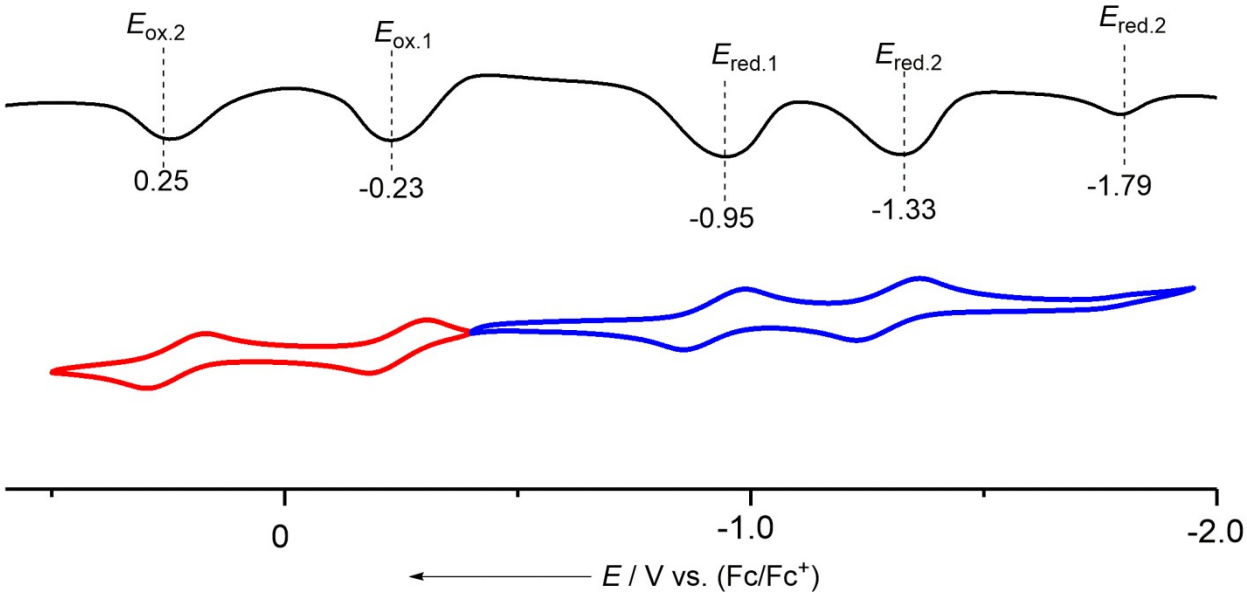

Figure S31. Cyclic voltammogram and differential pulse voltammogram of **$3Pd_2$**.

DFT Calculation

All calculations were carried out using the Gaussian 09 program.[2] All structures were fully optimized without any symmetry restriction. Geometries of **3**, **3HCl** and **$3Pd_2$** were optimized with the crystal structure of **3**, **3HCl** and **$3Pd_2$** as the starting structure at the density functional theory (DFT) method with B3LYP (Becke's three-parameter hybrid exchange functionals and the Lee-Yang-Parr correlation functional) level[3,4] while geometries of **3a** and **3b** were optimized with initial of their chemdraw 3D structures. In order to quantify the impact of the geometric change on aromaticity, a popular aromaticity index, the nucleus-independent chemical shifts (NICS) values were obtained with the GIAO method based on the final optimized structures. The global ring centers for the NICS values were designated at the nonweighted means of the carbon and nitrogen coordinates on the peripheral positions of conjugated macrocycles. Results for NICS(0), were collected, as shown in Fig. S49-S51. Here, NICS(0) is the NICS index at the geometric or areal center.

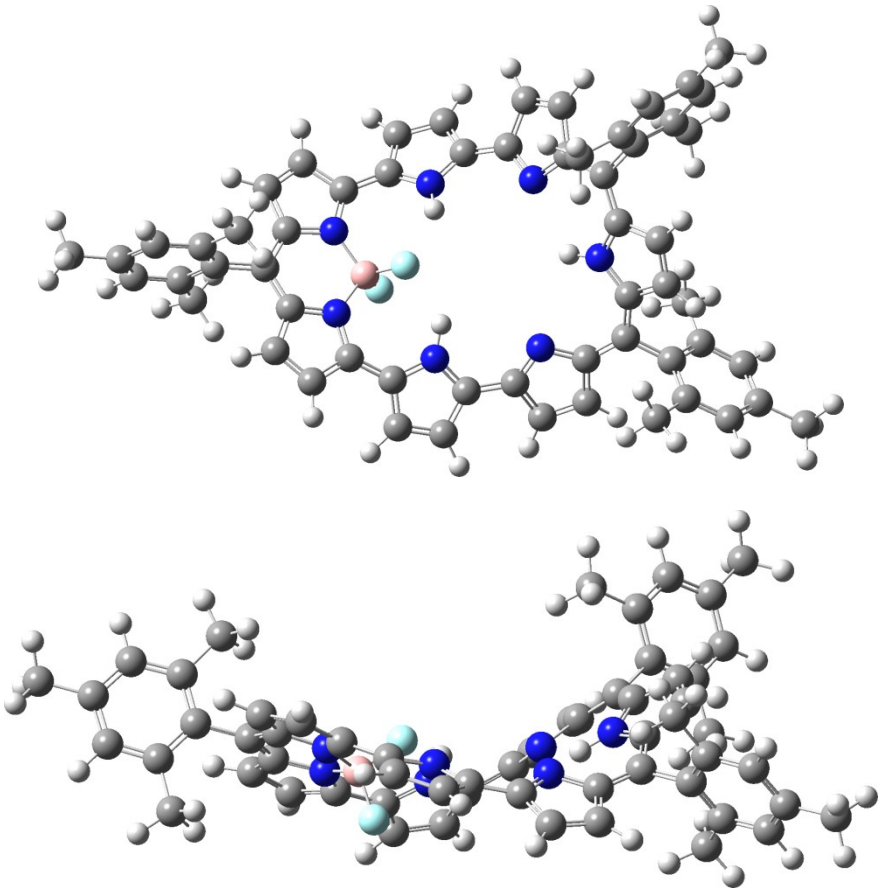

Figure S32 Optimized structure of **$3BF_2$** calculated at the (B3LYP/6-31G(d)) level.

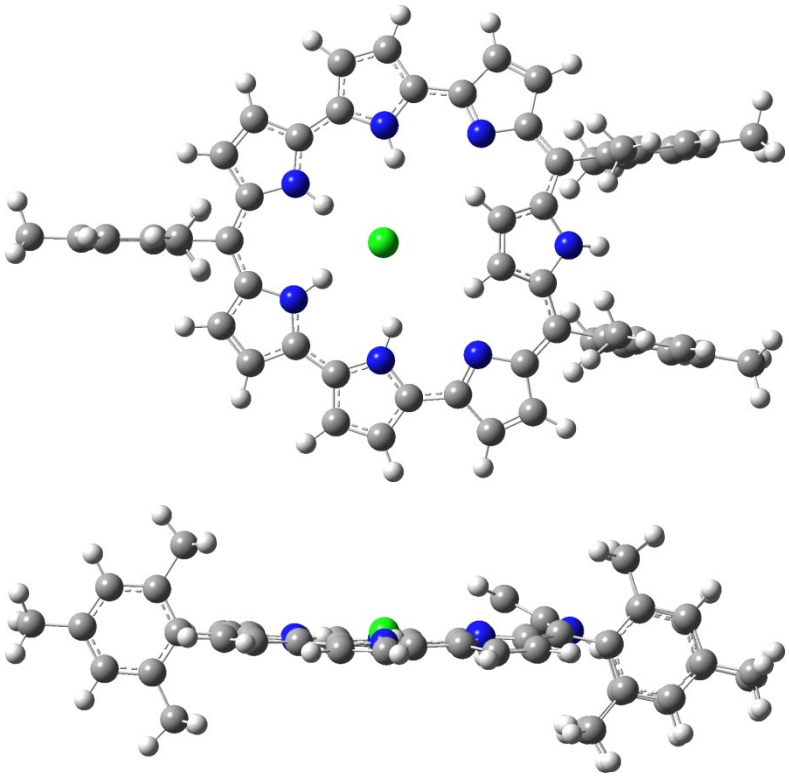

Figure S33 Optimized structure of **3HCl** calculated at the (B3LYP/6-31G(d)) level.

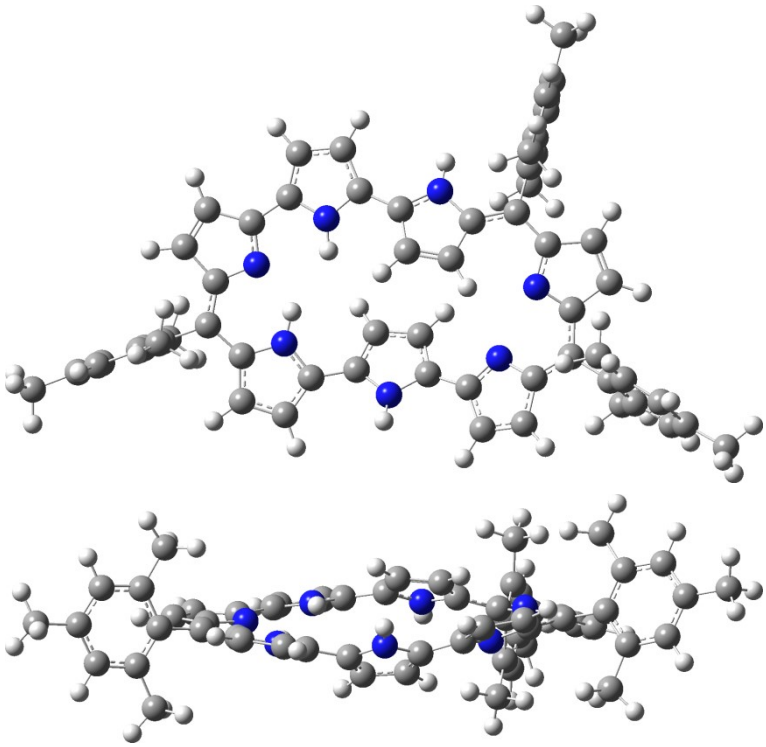

Figure S34 Optimized structure of **3a** calculated at the (B3LYP/6-31G(d)) level.

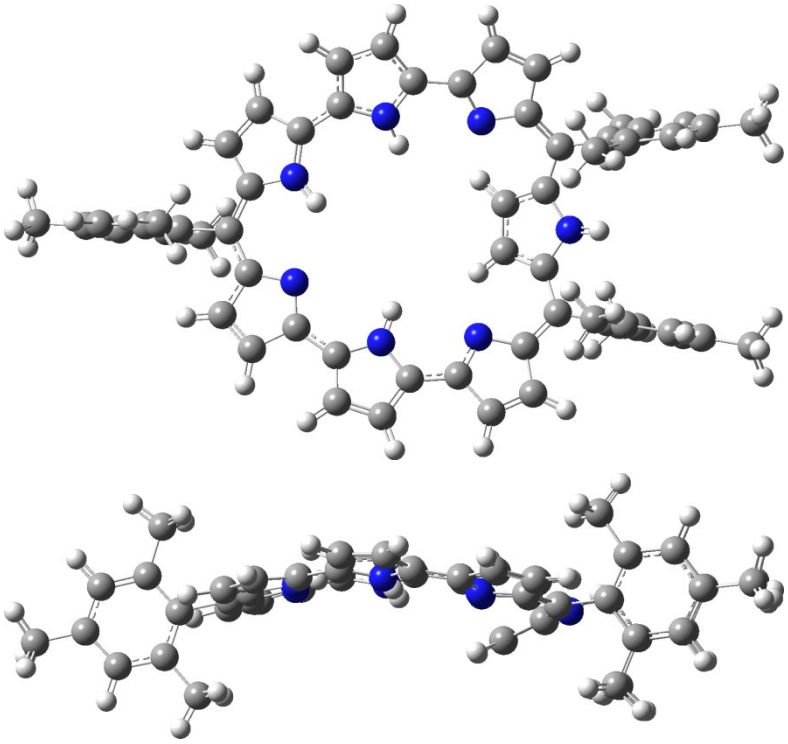

Figure S35 Optimized structure of **3b** calculated at the (B3LYP/6-31G(d)) level.

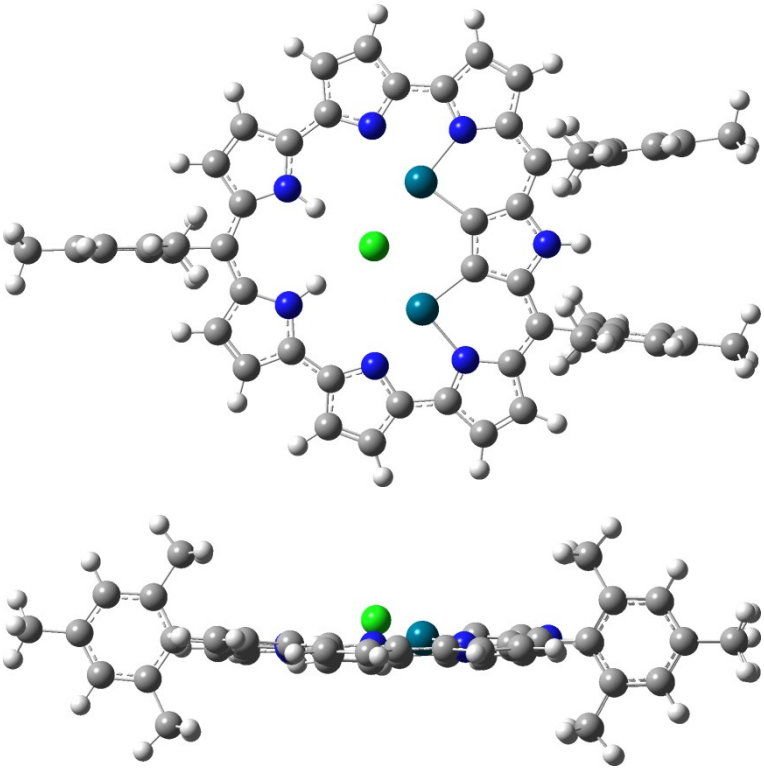

Figure S36 Optimized structure of **3Pd$_2$** calculated at the (B3LYP/6-31G(d)) level.

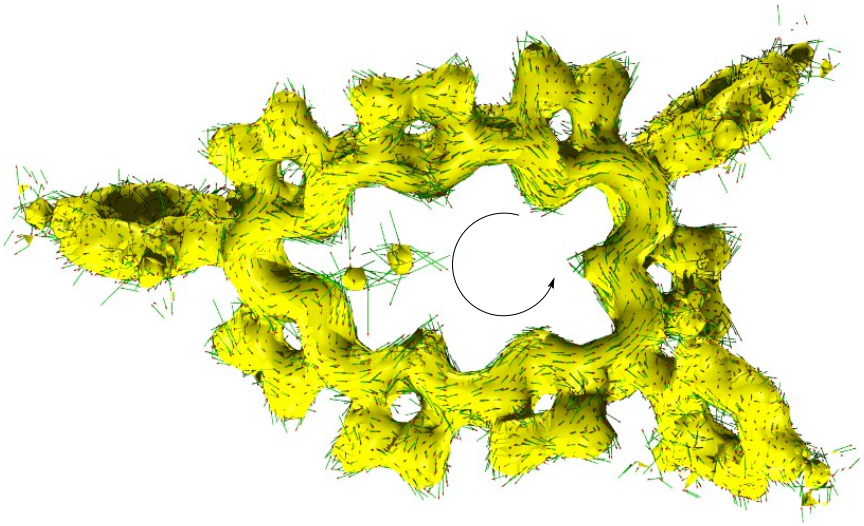

Figure S37 ACID plot of **3BF$_2$**.

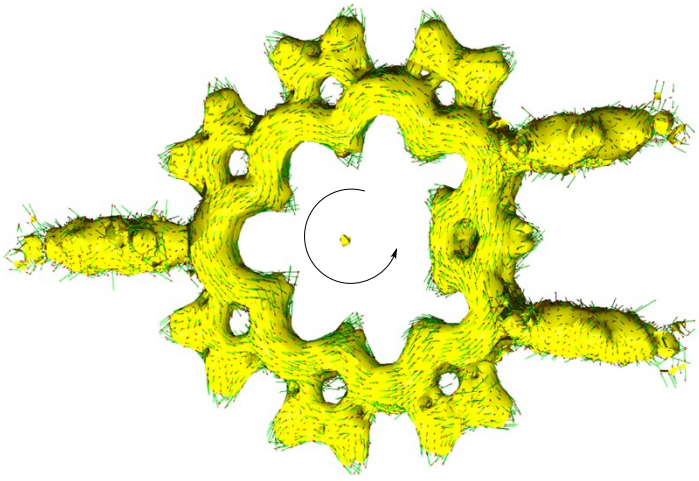

Figure S38 ACID plot of **3HCl**

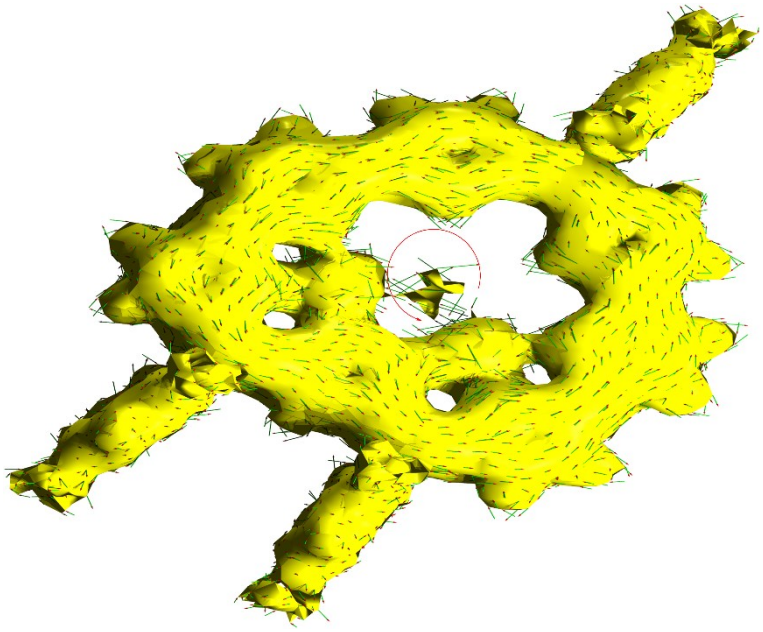

Figure S39 ACID plot of **3Pd$_2$**.

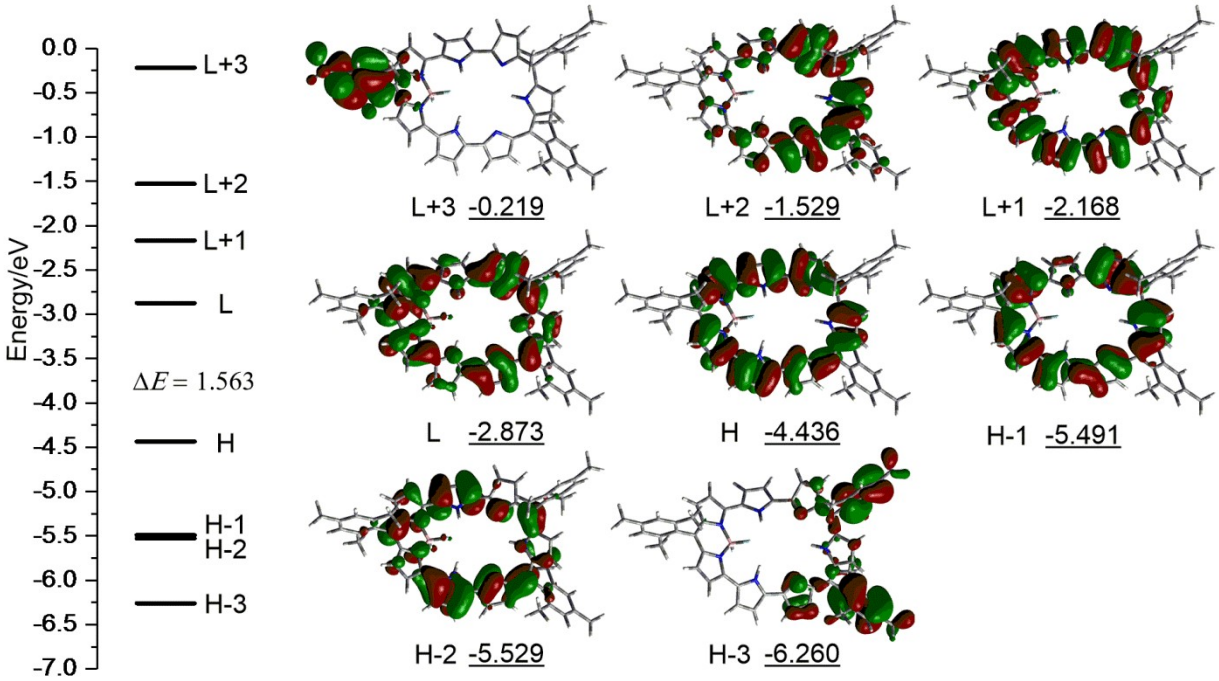

Figure S40 Frontier orbital diagrams of **3BF$_2$**.

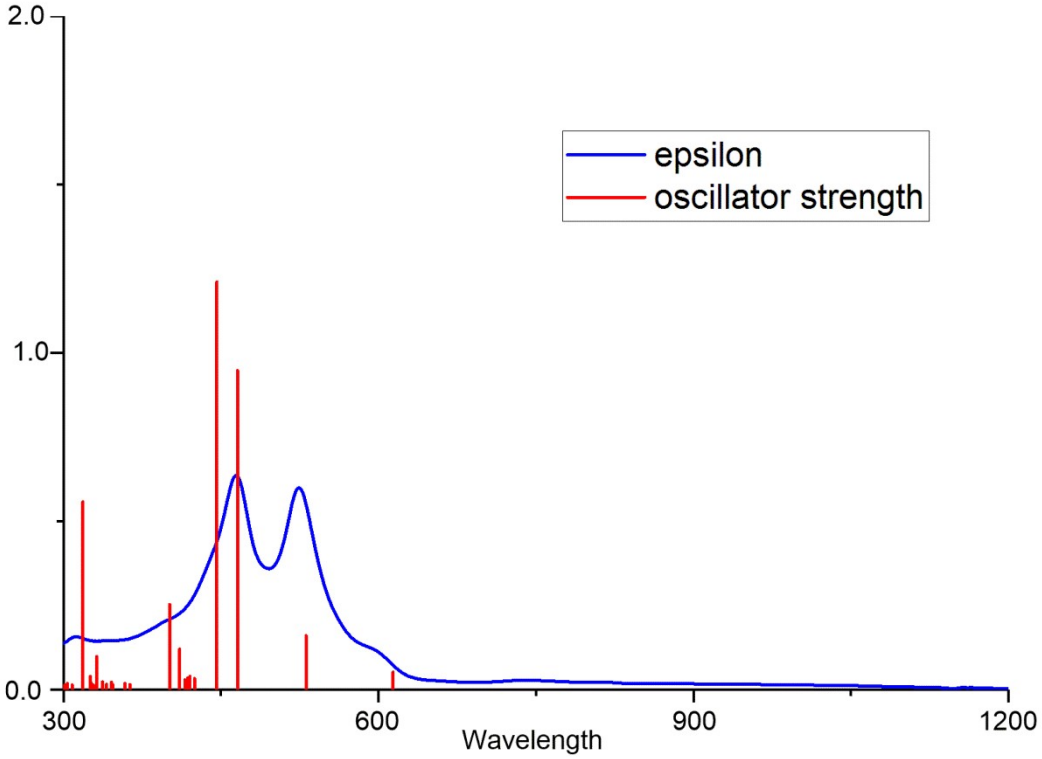

Wavelength (nm)	Oscillator Strengths	Major Transitions
614	0.0518	H -> L+1 70.2%, H-1 -> L 26.3%
531.19	0.1598	H-2 -> L 63.1%, H -> L+2 25.2%, H-1 -> L 9.8%
465.83	0.9472	H-1 -> L 58.6%, H -> L+1 29.3%, H-2 -> L 10.2%
446.1	1.2111	H -> L+2 67.6%, H-2 -> L 19.4%, H-8 -> L 5.3%
410.58	0.1202	H-1 -> L+1 73.4%, H-2 -> L+1 15.8%
401.11	0.2524	H-8 -> L 66.8%, H-2 -> L+1 19.2%
331.68	0.0981	H-18 -> L 73.3%, H-16 -> L 7.1%, H-4 -> L+1 5.4%
318.57	0.5579	H -> L+4 35.3%, H-16 -> L 16.9%, H-18 -> L 6.9%, H-1 -> L+2 5.7%, H-8 -> L+1 5.6%, H-17 -> L 5.3%, H -> L+7 5.3%
289.62	0.0505	H-5 -> L+2 34.8%, H-14 -> L+1 11.9%, H -> L+7 9.3%, H-6 -> L+2 7.3%, H-16 -> L+1 6.8%, H -> L+9 5.1%
287.67	0.0639	H-5 -> L+2 39.4%, H-8 -> L+2 12.3%, H -> L+7 7.6%

Figure S41 Calculated vertical transitions and major transitions of **3BF$_2$**.

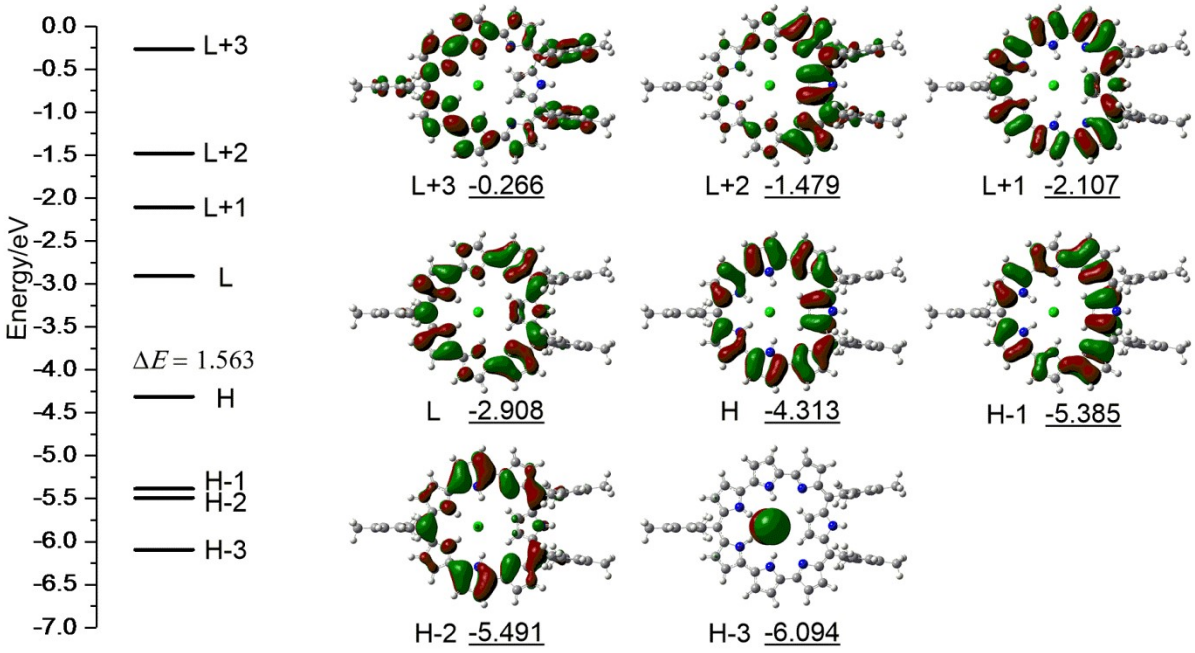

Figure S42 Frontier orbital diagrams of **3HCl**.

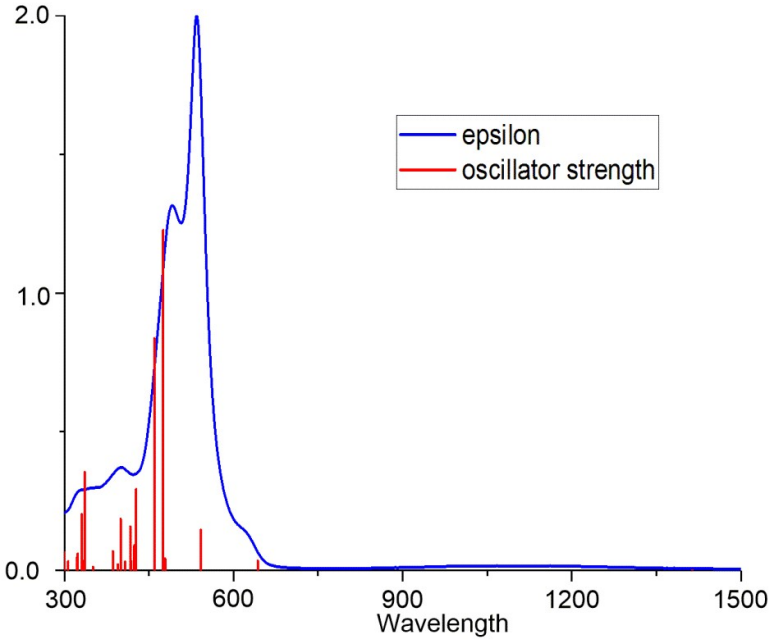

Wavelength (nm)	Oscillator Strengths	Major Transitions
542.08	0.1466	H-2 -> L 71.1%, H -> L+2 26.2%
475.09	1.2266	H-1 -> L 55.6%, H -> L+1 34.5%, H-4 -> L 8.4%

459.56	0.8366	H -> L+2 59.2%, H-2 -> L 20.9%, H-3 -> L 9.0%
427.15	0.2927	H-4 -> L 72.1%, H-5 -> L 12.1%, H-1 -> L 5.5%
423.98	0.0907	H-12 -> L 49.6%, H-6 -> L 27.0%, H-11 -> L 12.7%
416.75	0.1582	H-2 -> L+1 33.0%, H-6 -> L 32.9%, H-12 -> L 19.6%
399.61	0.1861	H-8 -> L 79.0%, H-2 -> L+1 6.1%
385.92	0.0694	H-17 -> L 47.9%, H-15 -> L 38.5%
336.22	0.3541	H -> L+3 60.4%, H-20 -> L 24.4%, H -> L+4 6.0%
330.81	0.2021	H-6 -> L+1 73.6%, H -> L+3 7.4%
323.34	0.0603	H-21 -> L 19.2%, H-13 -> L+1 18.6%, H-19 -> L 17.4%, H -> L+10 15.2%, H-2 -> L+2 9.9%
300.19	0.0644	H-20 -> L 20.4%, H-4 -> L+2 20.0%, H -> L+9 9.6%, H -> L+6 8.2%, H -> L+3 6.9%, H -> L+7 5.9%

Figure S43 Calculated vertical transitions and major transitions of **3HCl**.

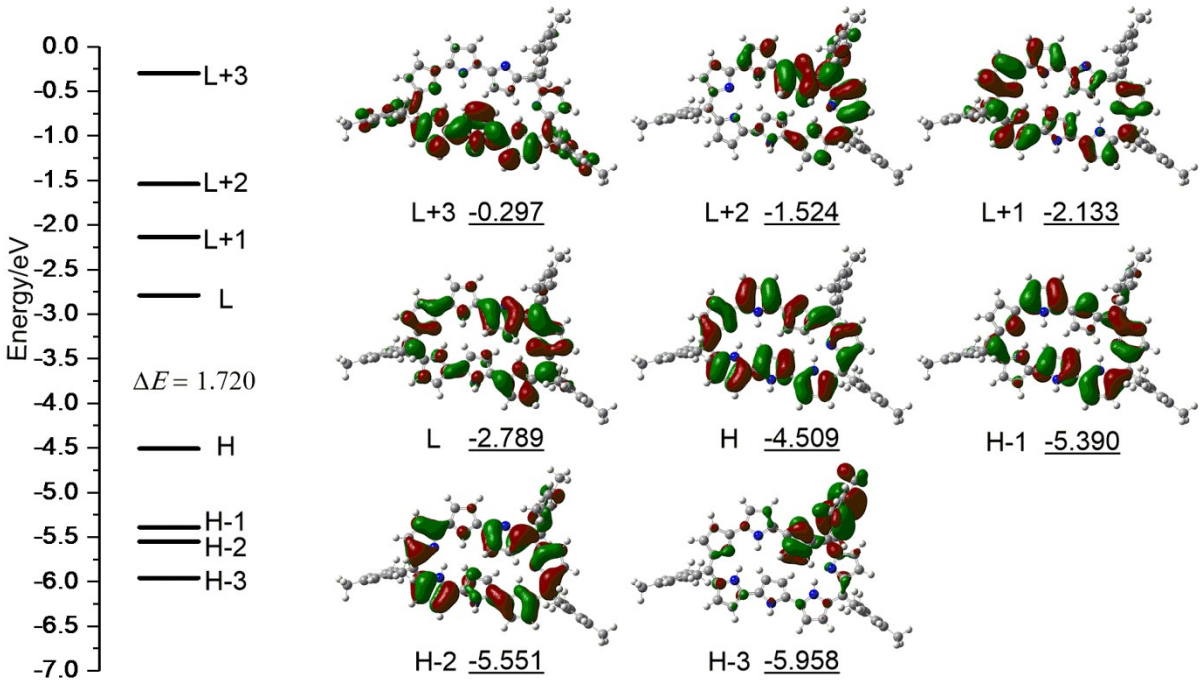

Figure S44 Frontier orbital diagrams of **3a**.

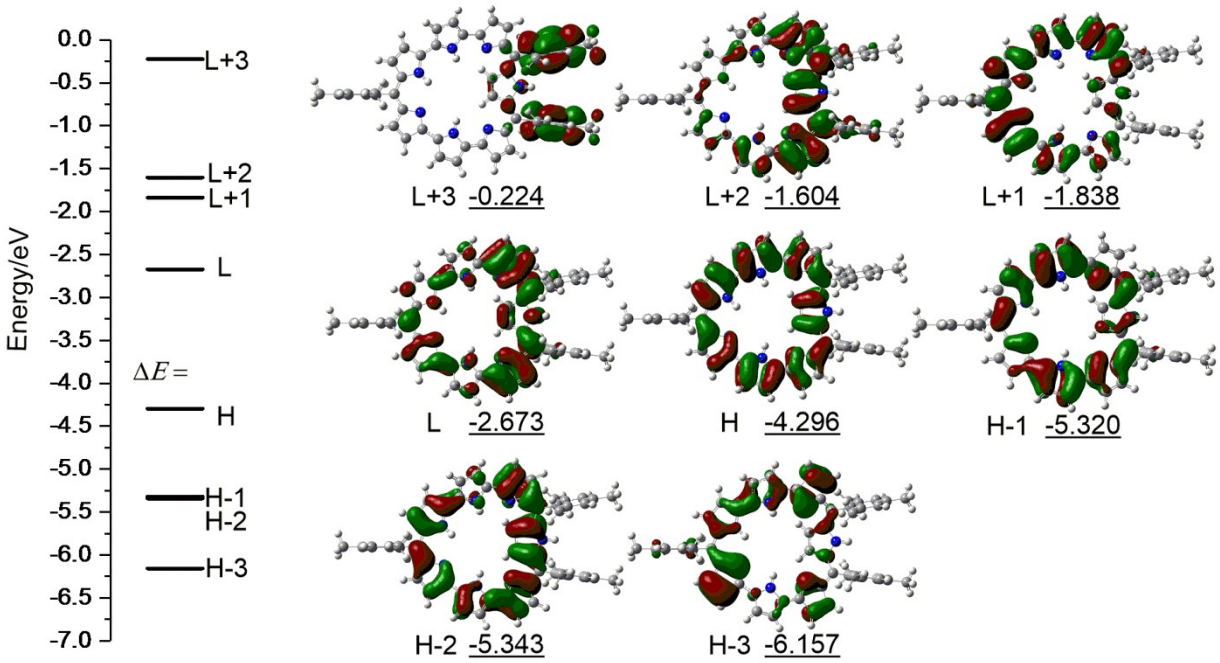

Figure S45 Frontier orbital diagrams of **3b**.

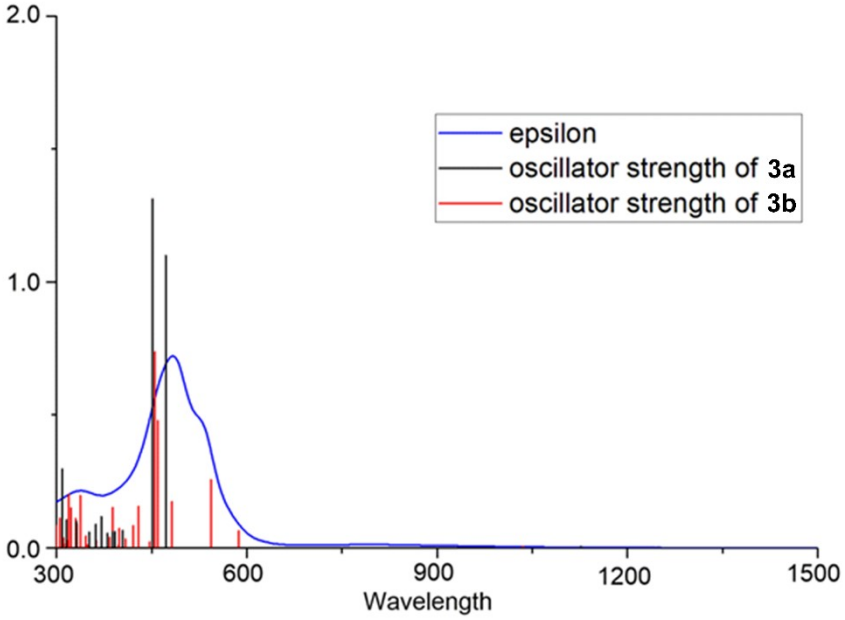

3a:

Wavelength (nm)	Oscillator Strengths	Major Transitions
587.49	0.0632	H -> L+1 70.7%, H-1 -> L 14.8%, H-2 -> L 12.5%
543.39	0.2567	H-1 -> L 63.5%, H -> L+2 15.4%, H-2 -> L 11.6%, H -> L+1 7.3%
482.13	0.1732	H-3 -> L 44.3%, H-2 -> L 36.2%, H -> L+1 10.5%

459.49	0.4777	H-3 -> L 49.4%, H-2 -> L 31.4%, H -> L+1 10.6%
455.41	0.7362	H -> L+2 70.4%, H-5 -> L 9.2%, H-1 -> L 8.0%, H-2 -> L 5.6%
428.91	0.1557	H-1 -> L+1 64.1%, H-5 -> L 22.2%
420.94	0.0838	H-5 -> L 60.1%, H-1 -> L+1 23.8%
398.96	0.0725	H-2 -> L+1 77.0%, H-1 -> L+2 6.8%
388.49	0.152	H-10 -> L 63.5%, H-7 -> L 11.7%, H-13 -> L 6.1%
337.23	0.1973	H-14 -> L 30.3%, H-19 -> L 15.2%, H-7 -> L+1 12.9%, H-2 -> L+2 8.0%, H-5 -> L+1 6.0%
331.76	0.0899	H-5 -> L+1 35.3%, H-7 -> L+1 19.5%, H-14 -> L 8.2%, H-10 -> L+1 6.7%, H-3 -> L+2 6.7%, H -> L+3 6.1%
329.9	0.1098	H-17 -> L 34.8%, H -> L+3 26.5%, H-16 -> L 23.0%, H-19 -> L 6.6%
322.81	0.15	H-18 -> L 60.4%, H-17 -> L 11.3%, H -> L+3 10.1%
319.44	0.2009	H -> L+3 23.2%, H-17 -> L 17.1%, H-10 -> L+1 10.7%, H-18 -> L 10.4%, H-14 -> L 6.0%, H-7 -> L+1 5.2%
315.46	0.0502	H-20 -> L 31.3%, H-10 -> L+1 15.6%, H-20 -> L+1 10.3%, H-18 -> L 7.5%, H-15 -> L 6.7%
305.12	0.1112	H-5 -> L+2 32.5%, H -> L+5 17.2%, H-16 -> L 11.4%, H -> L+3 8.9%, H -> L+4 8.8%, H-2 -> L+2 5.1%
299.60	0.0838	H-5 -> L+2 44.1%, H-16 -> L 14.1%, H-10 -> L+2 7.8%
285.67	0.0665	H-15 -> L+1 41.0%, H-14 -> L+1 36.1%, H -> L+8 11.5%

3b:

Wavelength (nm)	Oscillator Strengths	Major Transitions
1126.41	0.0053	H -> L 99.4%

472.05	1.0982	H -> L+2 49.7%, H-1 -> L 35.6%, H-2 -> L 6.9%
451.38	1.3117	H-2 -> L 52.5%, H -> L+1 33.1%, H-1 -> L 5.8%
404.05	0.0655	H-1 -> L+1 46.7%, H-5 -> L 29.0%, H-2 -> L+2 9.8%, H-6 -> L 6.6%
392.03	0.0613	H-2 -> L+1 67.1%, H-1 -> L+2 21.5%
388.3	0.0609	H-7 -> L 37.6%, H-12 -> L 29.5%, H-9 -> L 8.4%, H-11 -> L 7.0%
380.53	0.0543	H-7 -> L 41.6%, H-8 -> L 24.0%, H-9 -> L 11.1%, H-12 -> L 10.3%
370.59	0.1174	H-9 -> L 56.1%, H-11 -> L 13.4%, H-12 -> L 6.6%, H-2 -> L+2 6.1%, H-10 -> L 5.7%
362.06	0.0889	H-2 -> L+2 48.6%, H-12 -> L 18.4%, H-1 -> L+1 9.6%
351.41	0.0596	H-17 -> L 56.1%, H-15 -> L 11.5%, H-13 -> L 6.8%, H-19 -> L 6.5%
331.63	0.0992	H -> L+4 93.4%
315.67	0.1056	H -> L+6 89.2%
309.21	0.2967	H -> L+8 54.1%, H-18 -> L 26.4%, H-20 -> L 6.8%
296.15	0.0661	H-7 -> L+1 45.5%, H -> L+9 19.3%, H-3 -> L+2 9.2%, H-7 -> L+2 7.8%, H-8 -> L+1 5.6%
290.95	0.0617	H-7 -> L+2 20.6%, H-12 -> L+1 15.8%, H-18 -> L 13.6%, H -> L+8 9.3%, H-11 -> L+1 6.7%, H-12 -> L+2 5.3%
284.66	0.0546	H-10 -> L+2 22.1%, H-12 -> L+2 18.7%, H-9 -> L+1 15.1%, H-8 -> L+1 7.4%, H-10 -> L+1 6.5%, H-11 -> L+2 5.0%

Figure S46 Calculated vertical transitions and major transitions of **3a** and **3b**.

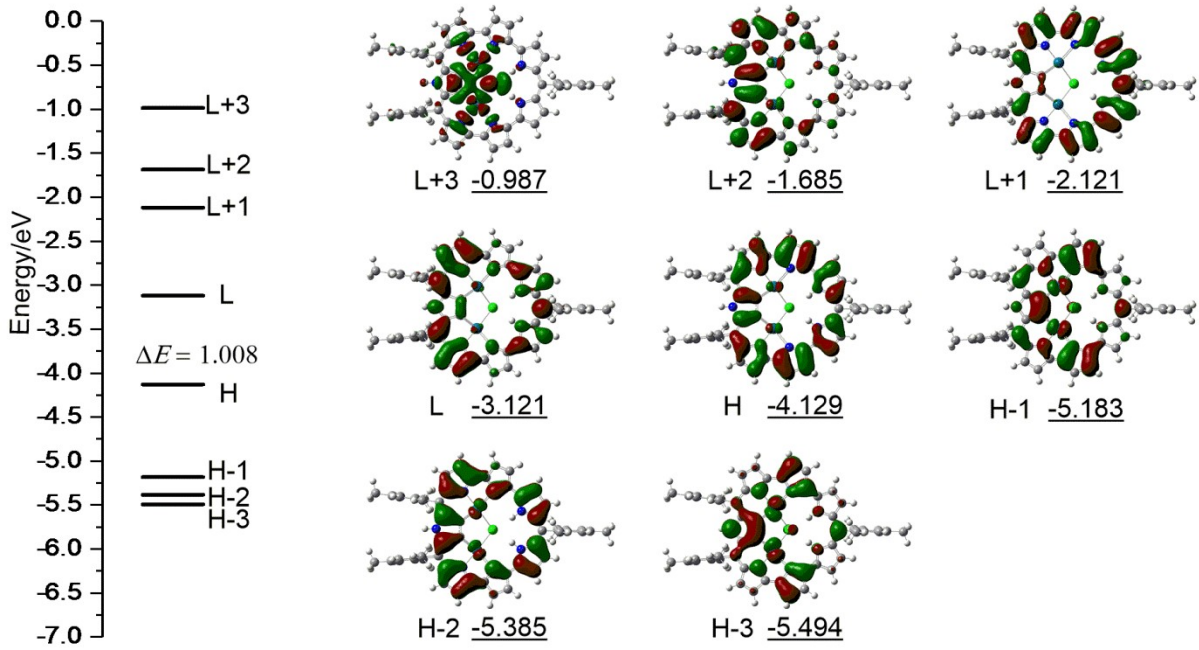

Figure S47 Frontier orbital diagrams of **3Pd$_2$**.

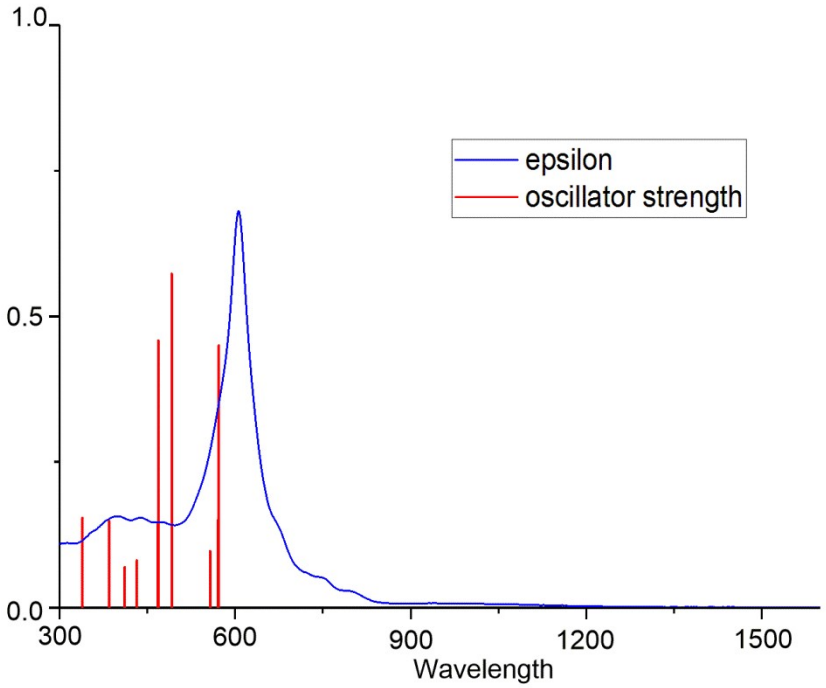

Wavelength (nm)	Oscillator Strengths	Major Transitions
572.31	0.4505	H-2 -> L 40.6%, H -> L+1 30.8%, H-8 -> L 20.1%
570.59	0.1503	H -> L+2 50.8%, H-5 -> L 33.8%, H-3 -> L 7.9%
557.51	0.0973	H-5 -> L 44.4%, H-7 -> L 35.5%, H -> L+2 11.1%
491.77	0.5735	H-7 -> L 54.6%, H-5 -> L 14.6%,

		H-3 -> L 11.8%, H -> L+2 7.6%, H-1 -> L+1 5.6%
468.61	0.4589	H-8 -> L 64.3%, H-1 -> L+1 10.0%, H-2 -> L 8.4%, H -> L+1 7.3%
468.15	0.1455	H-1 -> L+1 74.5%, H-8 -> L 8.5%, H-3 -> L+1 5.6%
432.18	0.0812	H-2 -> L+1 67.2%, H-1 -> L+2 20.9%
411.1	0.0696	H-1 -> L+2 63.9%, H-2 -> L+1 17.7%, H-3 -> L+2 5.9%, H-17 -> L 5.2%
385.16	0.1410	H-2 -> L+2 72.9%, H-3 -> L+1 5.0%
384.61	0.1484	H-3 -> L+2 72.6%
338.99	0.1545	H-21 -> L 31.9%, H-23 -> L 14.2%, H -> L+9 14.0%, H-9 -> L+1 12.4%, H-19 -> L 10.2%, H-20 -> L 7.5%

Figure S48 Calculated vertical transitions and major transitions of **3Pd$_2$**.

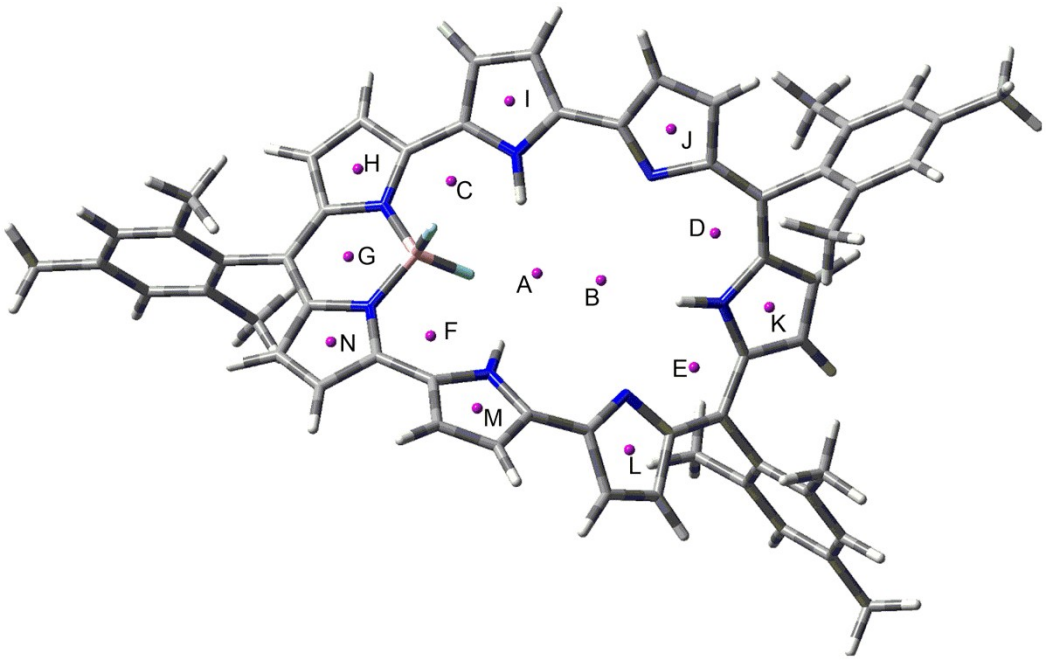

NO.	NICS(0) Value / ppm	NO.	NICS(0) Value / ppm
A	9.3887	**I**	-6.6551
B	9.8388	**J**	-2.4172
C	11.4535	**K**	-4.3657
D	12.9277	**L**	-2.4746
E	13.8580	**M**	-6.7319
F	11.8464	**N**	-2.2739
G	14.3586		
H	-2.4098		

Figure S49. NICS values of **3BF$_2$**.

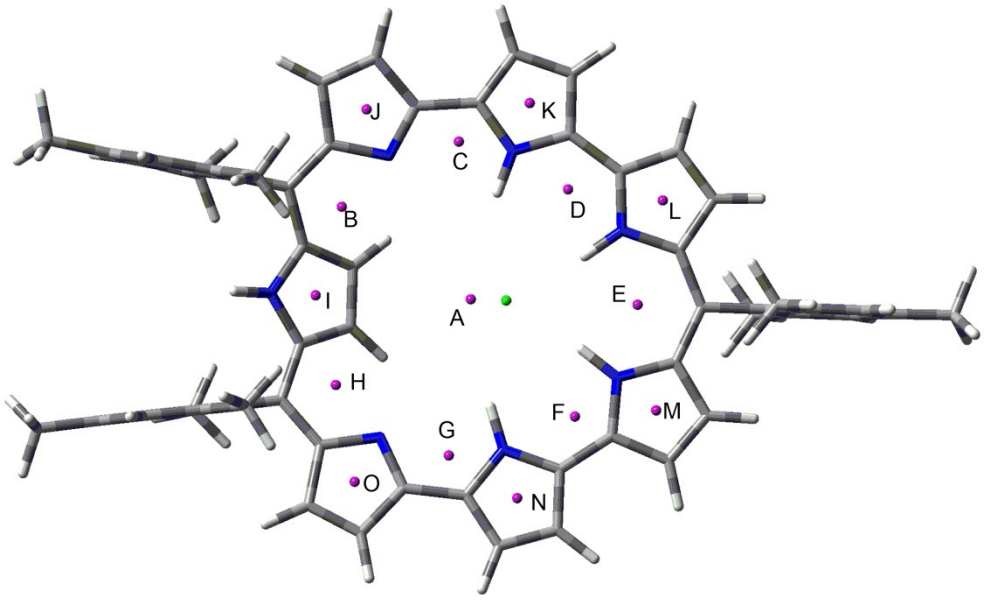

NO.	NICS(0) Value / ppm	NO.	NICS(0) Value / ppm
A	–	**I**	-3.2660
B	23.9614	**J**	-5.5253
C	18.5803	**K**	-3.9244
D	18.5684	**L**	-2.3897
E	21.2941	**M**	-2.1509
F	15.8311	**N**	-3.8032
G	18.6629	**O**	-5.6494
H	23.7110		

Figure S50. NICS values of **3HCl**. (Point A is too close to the Cl^-, so the value is meaningless)

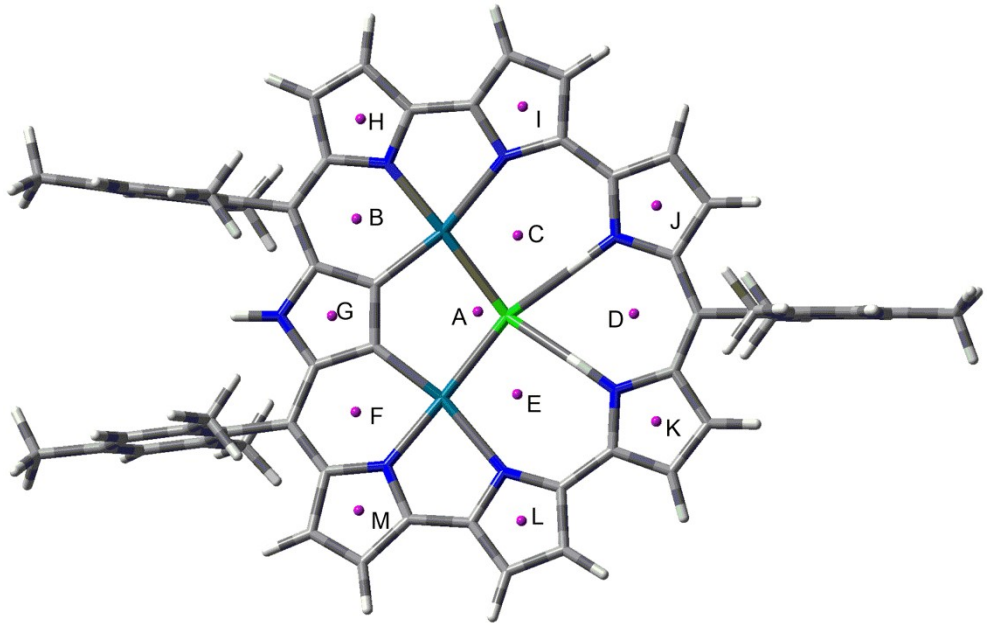

NO.	NICS(0) Value / ppm	NO.	NICS(0) Value / ppm
A	-	**I**	2.7398
B	64.1313	**J**	10.2367
C	35.9735	**K**	10.7401
D	54.0139	**L**	2.6380
E	35.8415	**M**	3.8024
F	64.4984		
G	18.2931		
H	3.5646		

Figure S51. NICS values of **3Pd$_2$**. (Point A is too close to the Cl^-, so the value is meaningless)

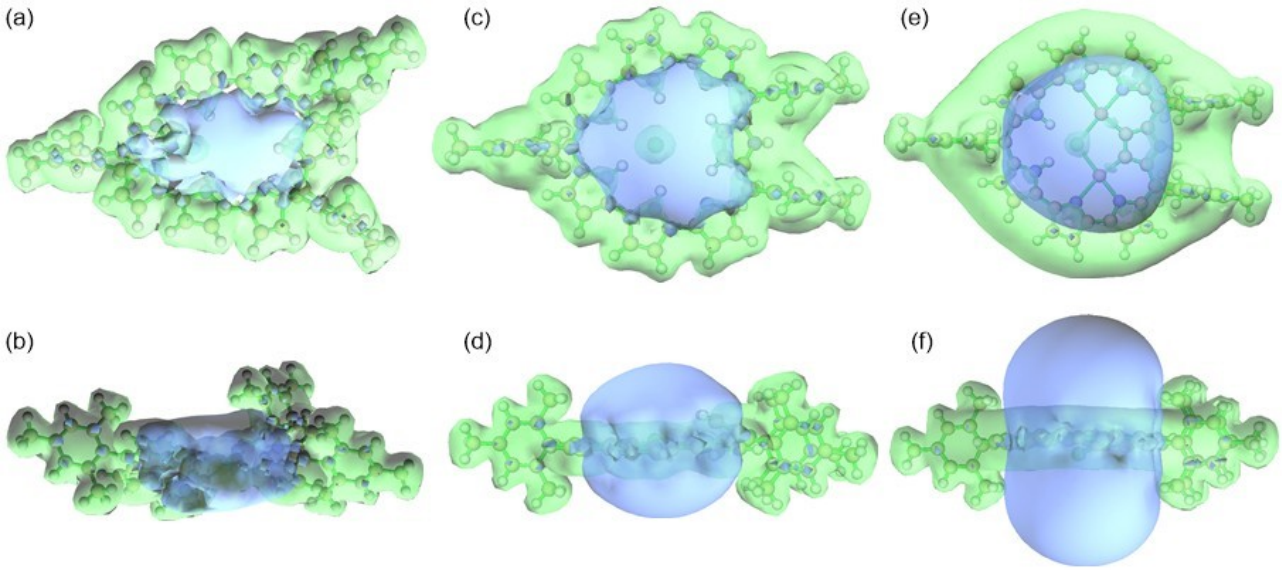

Figure S52. ICSS (iso-chemical shielding surfaces) of **3BF$_2$** a) topview b) sideview, **3HCl** c) topview d) sideview and **3Pd$_2$** e) topview f) sideview: The green isosurface represents the region with a magnetic shielding value of 5.0 ppm. The blue isosurface represents a shielding value of -5.0 ppm.

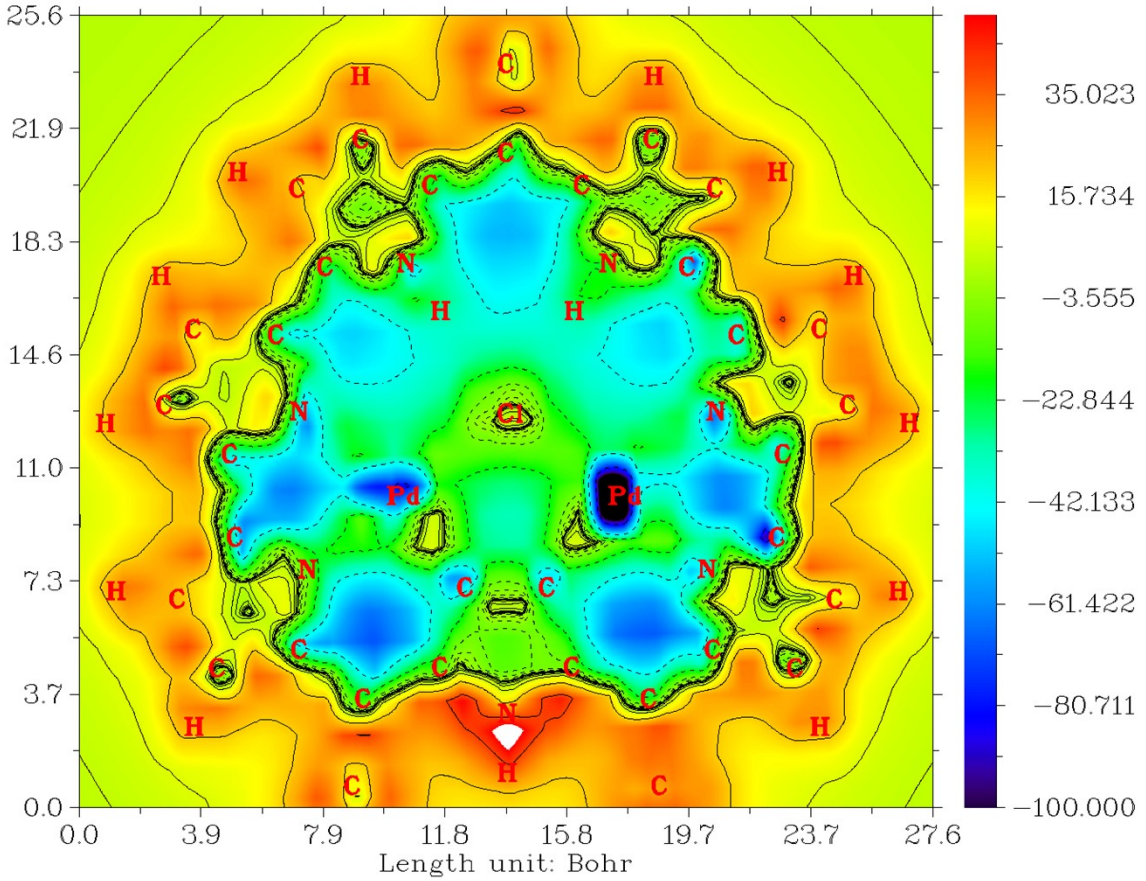

Figure S53. ICSS$_{ZZ}$(1) plotting of **3Pd$_2$**.

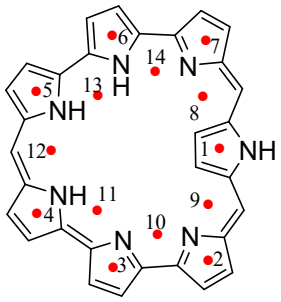

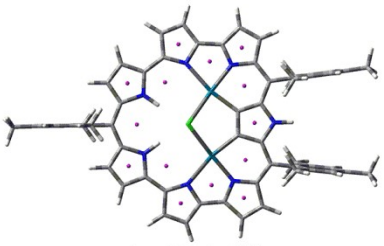

A: $3Pd_2Cl$

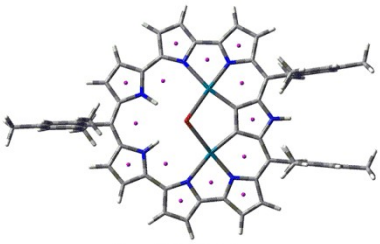

B: $3Pd_2Br$

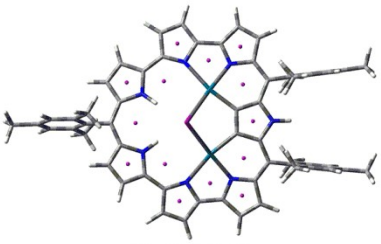

C: $3Pd_2I$

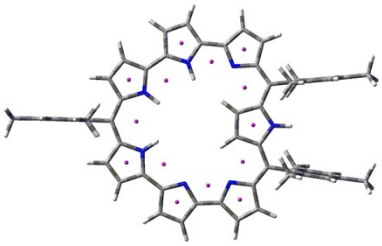

D: $3Pd_2Cl$-Pd_2Cl removal

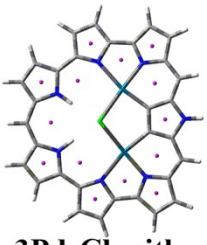

E: $3Pd_2Cl$-without substituents

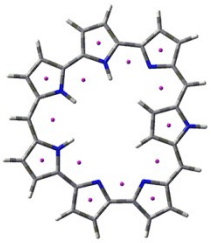

F: $3Pd_2Cl$-only macrocyle

	1	2	3	4	5	6	7	8	9	10	11	12	13	14
A	18.26	3.55	2.72	10.22	10.73	2.62	3.79	64.38	64.01	64.28	49.22	53.90	49.32	64.02
B	18.06	3.60	2.76	11.25	10.74	2.76	3.33	62.81	63.11	63.54	48.77	53.53	48.47	63.92
C	17.30	2.89	2.98	10.80	11.23	1.92	2.10	58.29	58.10	59.77	45.85	50.92	44.71	60.75
D	4.14	-12.08	-13.40	8.94	5.61	5.12	-6.84	47.82	49.24	46.83	37.68	39.69	35.13	42.33
E	22.80	5.03	3.71	13.68	13.36	3.83	4.79	75.02	75.26	74.84	57.65	62.57	57.57	75.14
F	5.36	-12.96	-14.90	10.29	7.03	6.66	-6.99	52.45	53.80	51.37	41.62	43.37	37.98	46.73

Figure S54. NICS values of related structures based on optimized structure of **$3Pd_2$** (with only atoms replacement).

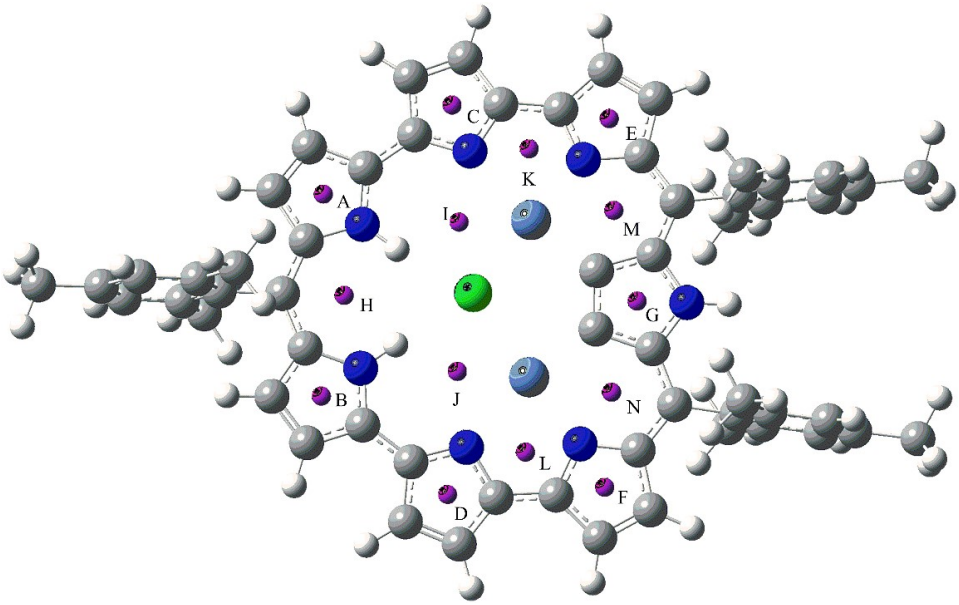

NO.	NICS(0) Value / ppm	NO.	NICS(0) Value / ppm
A	9.3367	**I**	37.7329
B	9.5017	**J**	37.8853
C	1.2241	**K**	57.1465
D	1.4203	**L**	57.0536
E	5.4271	**M**	56.8600
F	5.2876	**N**	56.7500
G	20.7420		
H	51.0344		

Figure S55. NICS values of **3Ni$_2$** based on optimized structure of **3Pd$_2$** (with only atoms replacement).

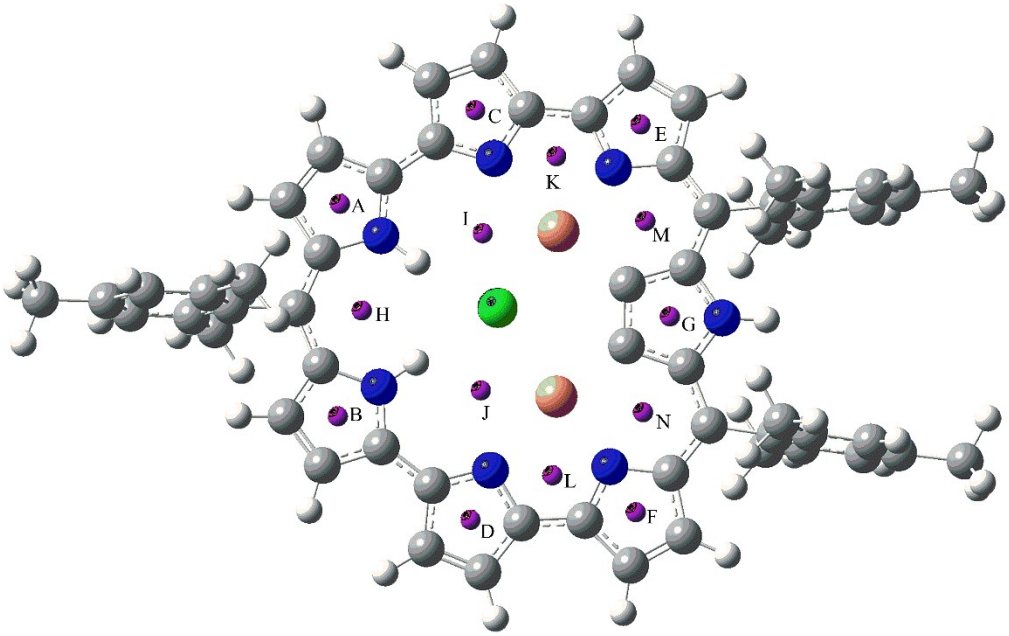

NO.	NICS(0) Value / ppm	NO.	NICS(0) Value / ppm
A	8.4032	**I**	33.0627
B	8.6067	**J**	33.1095
C	0.1331	**K**	55.8462
D	0.3653	**L**	55.8345
E	5.2907	**M**	56.5541
F	5.0907	**N**	56.4629
G	10.2577		
H	48.7123		

Figure S56. NICS values of **3Cu$_2$** based on optimized structure of **3Pd$_2$** (with only atoms replacement).

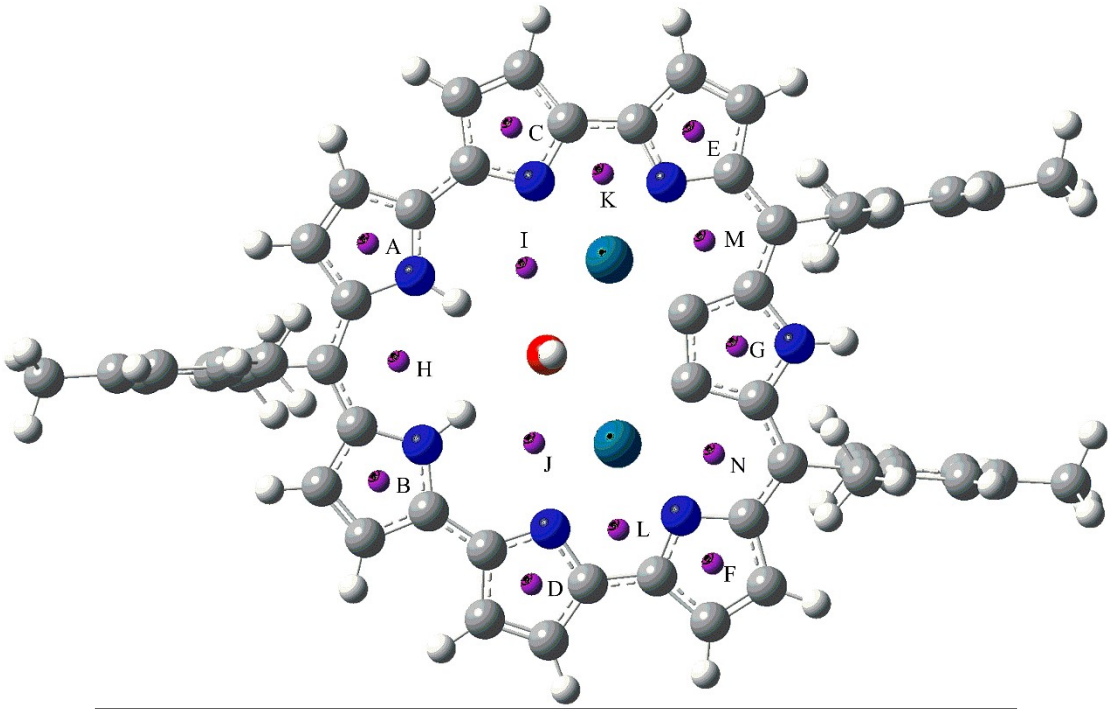

NO.	NICS(0) Value / ppm	NO.	NICS(0) Value / ppm
A	11.7338	**I**	39.7698
B	11.8924	**J**	39.8271
C	3.7297	**K**	67.9423
D	3.9758	**L**	67.7954
E	4.2337	**M**	66.5374
F	4.0815	**N**	66.3829
G	-20.6300		
H	57.6194		

Figure S57. NICS values of **3Pd$_2$-OH**.

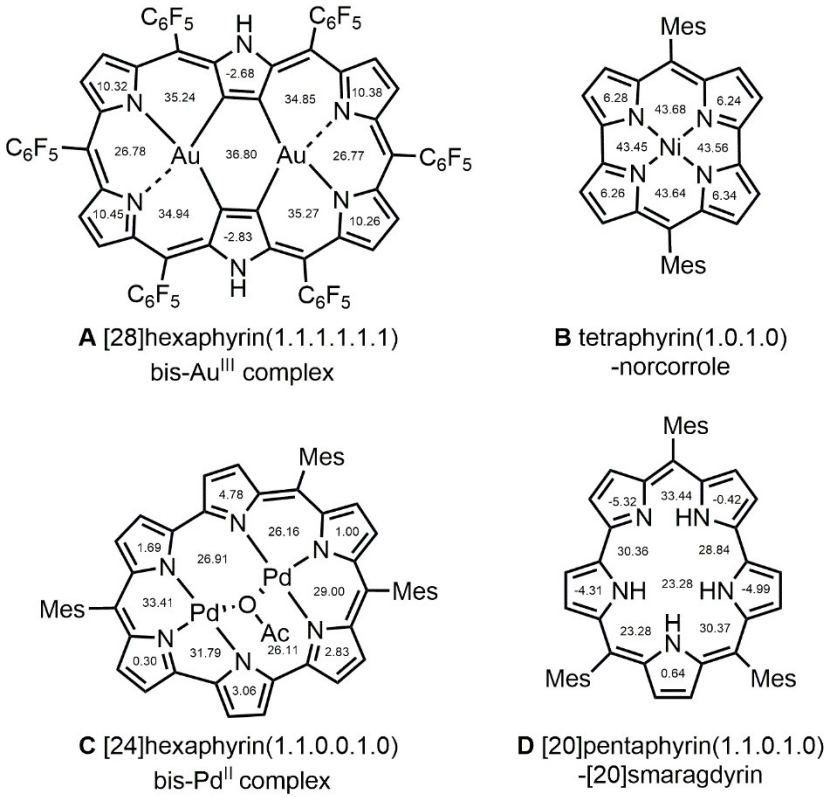

Figure S58 NICS values of **A**, **B**, **C** and **D** calculated at the (B3LYP/6-31G(d)) level.

Other experiments

Reduction of **$3BF_2$**:

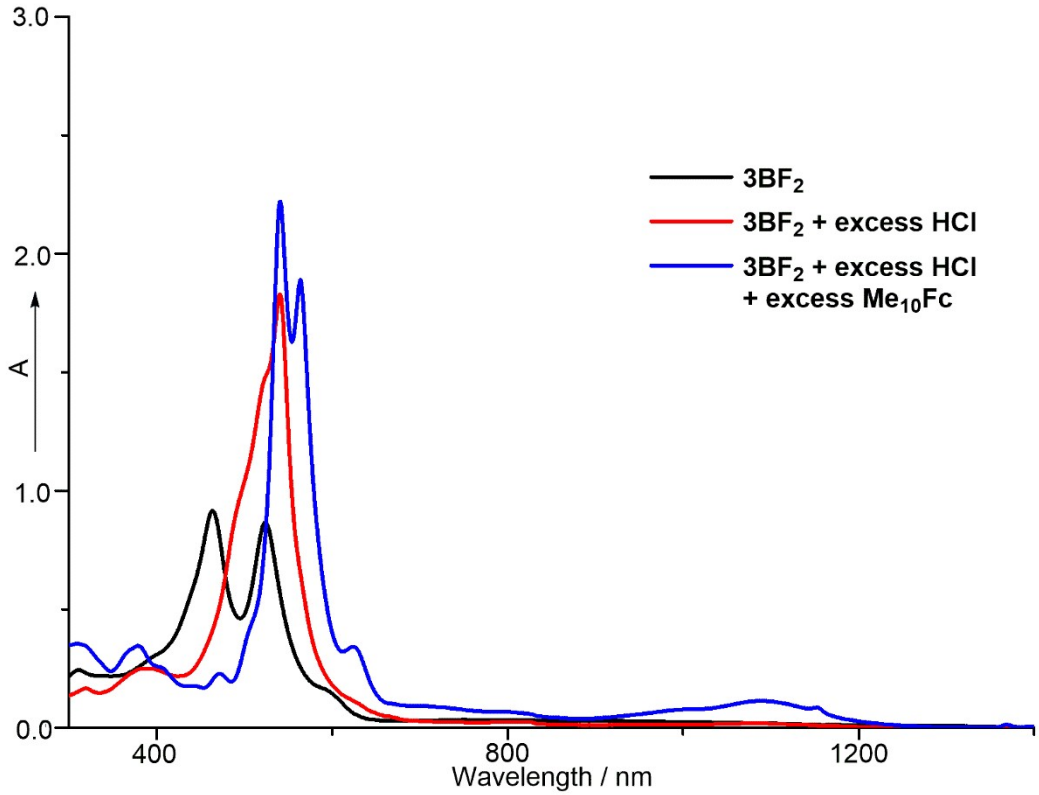

Figure S59. UV/Vis/NIR spectra of **$3BF_2$**, **$3BF_2$** treated with excess HCl and **$3BF_2$** treated with excess HCl & excess $Me_{10}Fc$ in CH_2Cl_2.

Oxidation of **3Pd**:

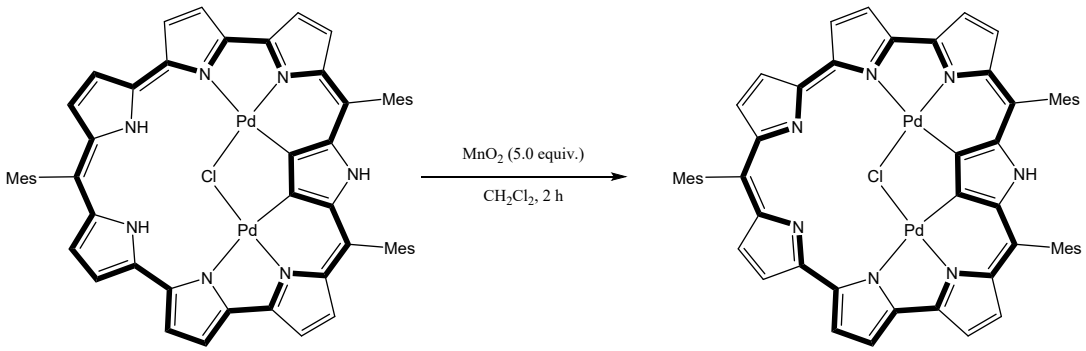

$3Pd_2$ **$3Pd_2$-Ox**

$3Pd_2$ (10.0 mg, 0.009 mmol) was dissolved in CH_2Cl_2 (5 mL) and MnO_2 (4.0 mg, 5.0 equiv. 0.046 mmol) was added. The mixture was stirred vigorously for 2 h and then purified by a Celite column (CH_2Cl_2 as an eluent). After evaporation of the solvent and recrystallization with hexane gave **$3Pd_2$-Ox** (5.2 mg, 52% yield) as a grey solid.

$3Pd_2$-Ox: ^{1}H NMR (500 MHz, Chloroform-*d*) δ = 11.25 (m, 2H, β-H), 11.10 (br, 2H, β-H), 10.67 (m, 2H, β-H), 10.27 (d, J = 4.3 Hz, 2H, β-H), 9.94 (br, 2H, β-H), 9.64 (d, J = 4.6, 2H, β-H), 8.10 (br, 1H, NH), 7.61 (s, 2H, Ar-H), 7.50 (s, 4H, Ar-H), 2.88 (s, 3H, Me-H), 2.68 (s, 6H, Me-H) and 2.08 (br, 18H, Me-H) ppm. HR-MS (MALDI-TOF-MS): *m/z* = 1088.1606, calcd for $(C_{58}H_{46}ClN_7Pd_2)^+$ = 1088.1668 ($[M+H]^+$); λ_{max} (ε [$M^{-1}cm^{-1}$]) = 464 (52000), 627 (115900), 784 (10600), 899 (14000), 1020 (17000) and 1200 (3000) nm.

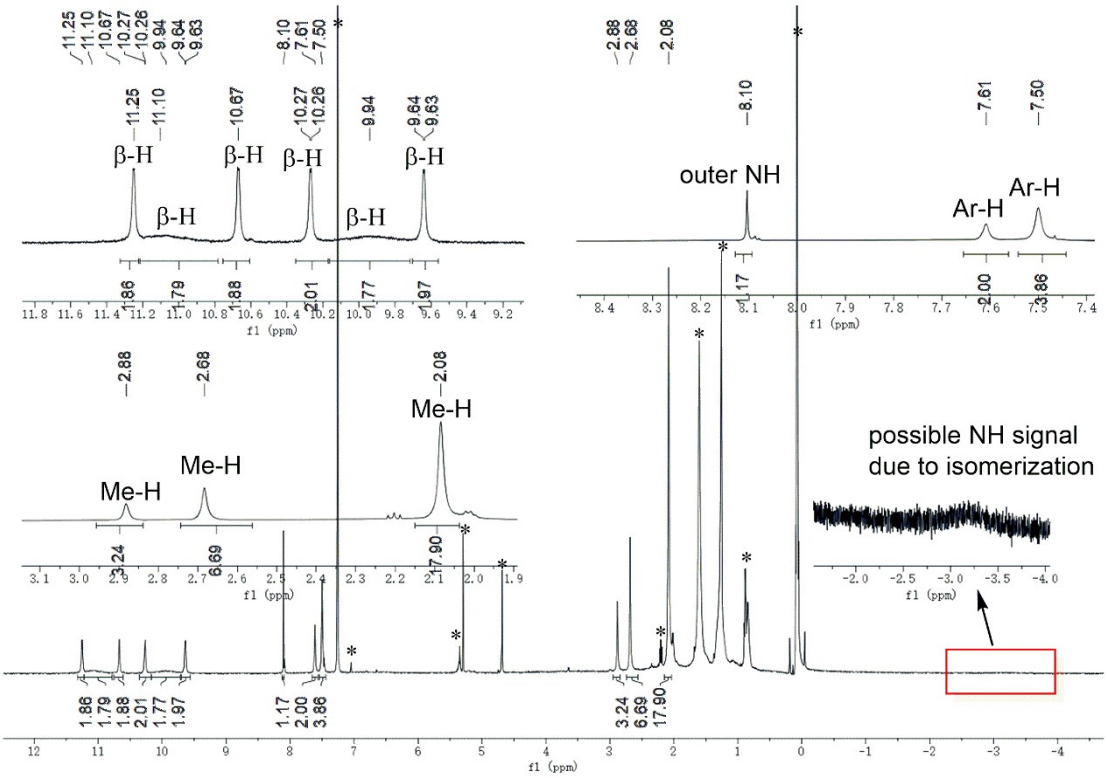

Figure S60. ^{1}H NMR spectrum of **3Pd$_2$-Ox** in $CDCl_3$ at 298K. Asterisk means residual solvent or impurity.

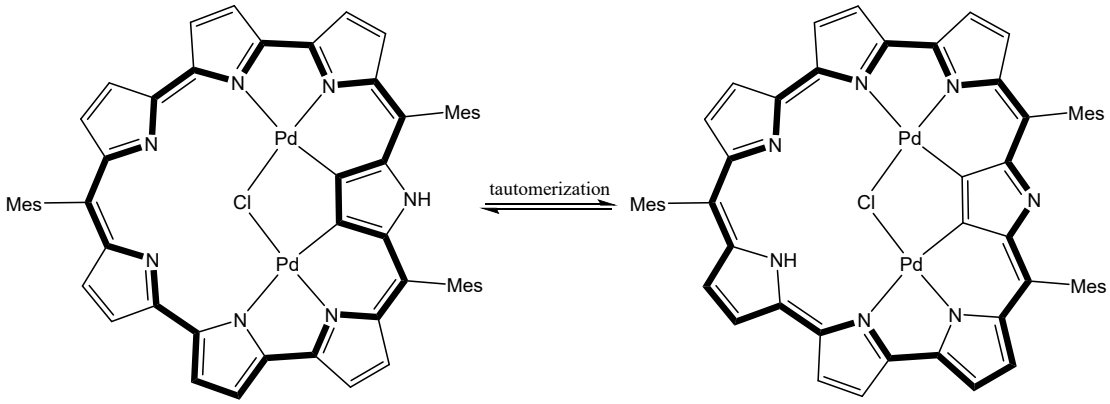

3Pd$_2$-Ox-a **3Pd$_2$-Ox-b**

Figure S61. Possible tautomerization between **3Pd$_2$-Ox-a** and **3Pd$_2$-Ox-b**.

Broad peaks at 11.10 ppm and 9.94 ppm due to the β-protons and those in a range of -2.5 to -3.5 ppm might be ascribed to tautomerization between **3Pd$_2$-Ox-a** and **3Pd$_2$-Ox-b** indicated below.

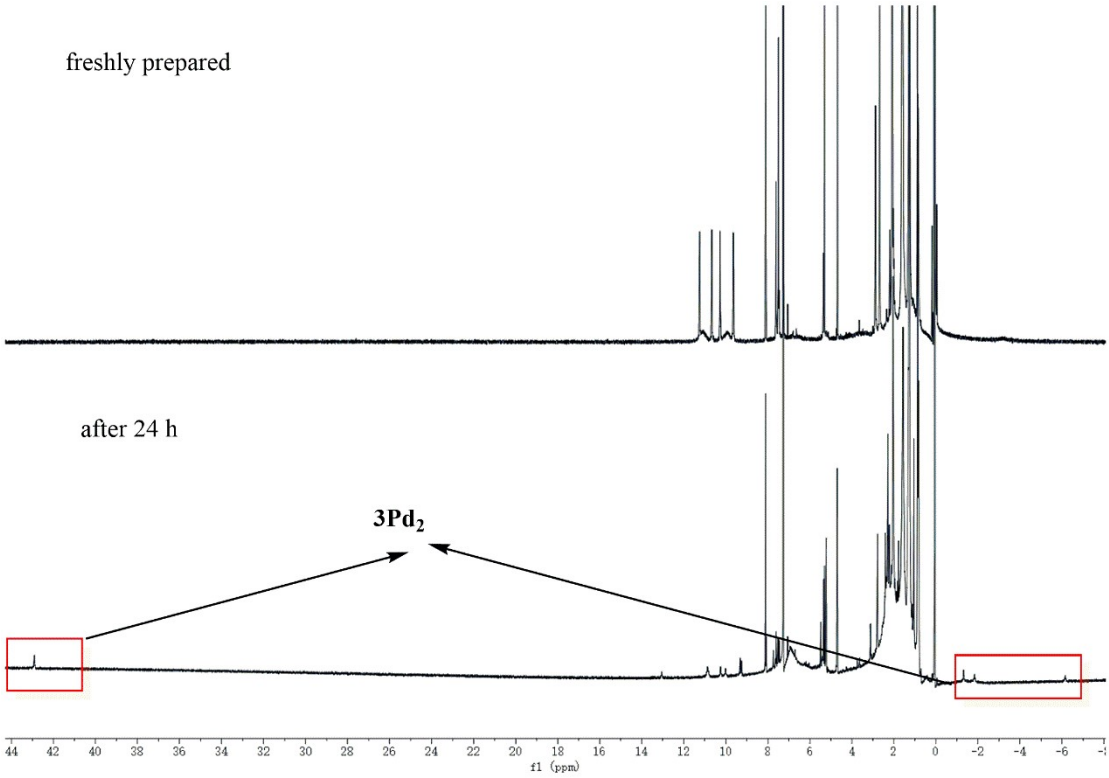

Figure S62. ^{1}H NMR spectrum of **3Pd$_2$-Ox** in $CDCl_3$ at 298K (freshly prepared and after 24 h).

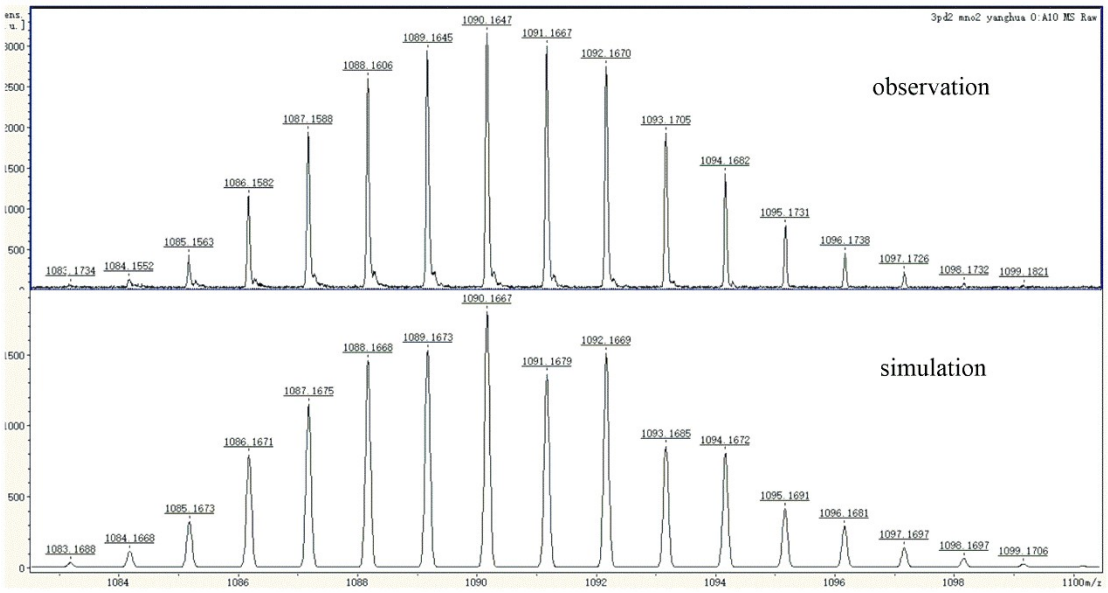

Figure S63. MS spectrum of **3Pd$_2$-Ox**.

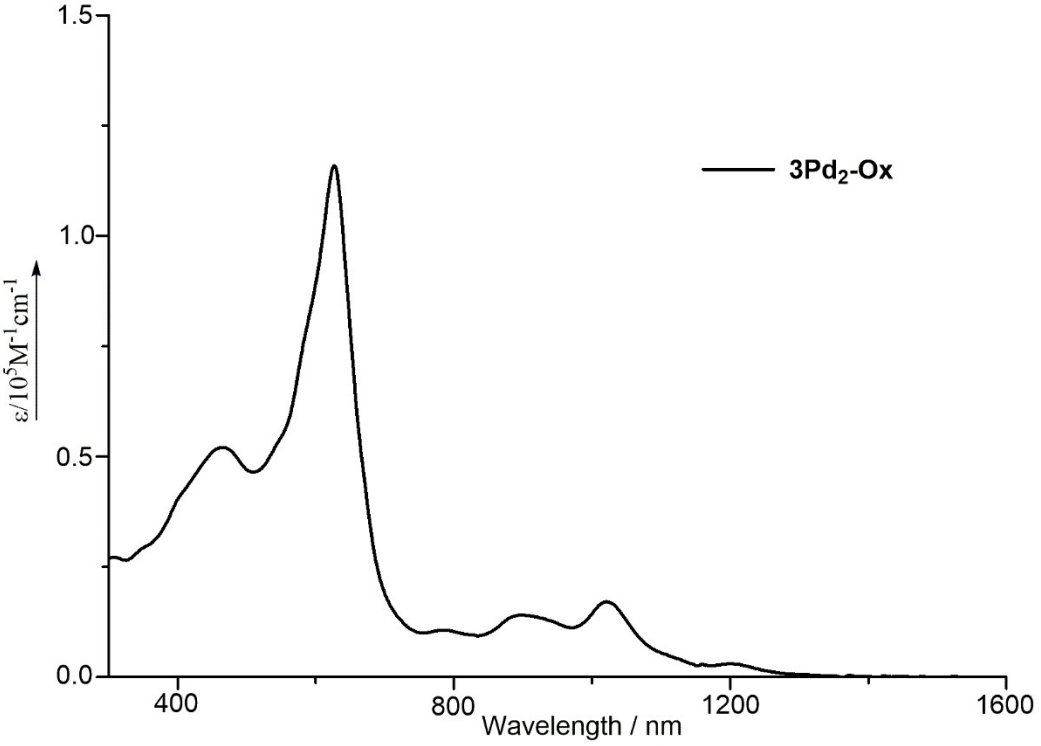

Figure S64. UV/Vis/NIR absorption spectrum of **$3Pd_2$-Ox** in CH_2Cl_2.

Supporting References

[1] M. Umetani, J. Kim, T. Tanaka, D. Kim, A. Osuka. 5,20-Diheterohexaphyrins: Metal Template Free Synthesis and Aromaticity Switching. *Chem. Commun.* **2019**, *55*, 10547.

[2] Gaussian 09,Revision A.02, M.J. Frisch, G.W. Trucks, H. B. Schlegel, G. E. Scuseria, M. A. Robb, J. R. Cheeseman, G. Scalmani, V. Barone, B. Mennucci, G. A. Petersson, H. Nakatsuji, M. Caricato, X. Li, H. P. Hratchian, A. F. Izmaylov, J. Bloino, G. Zheng, J. L. Sonnenberg, M. Hada, M. Ehara, K. Toyota, R. Fukuda, J. Hasegawa, M. Ishida, T. Nakajima, Y. Honda, O. Kitao, H. Nakai, T. Vreven, J. A. Montgomery, Jr., J. E. Peralta, F. Ogliaro, M. Bearpark, J. J. Heyd, E. Brothers, K. N. Kudin, V. N. Staroverov, R. Kobayashi, J. Normand, K. Raghavachari, A. Rendell, J. C. Burant, S. S. Iyengar, J. Tomasi, M. Cossi, N. Rega, J. M. Millam, M. Klene, J. E. Knox, J. B. Cross, V. Bakken, C. Adamo, J. Jaramillo, R. Gomperts, R. E. Stratmann, O. Yazyev, A. J. Austin, R. Cammi, C. Pomelli, J. W. Ochterski, R. L. Martin, K. Morokuma, V. G. Zakrzewski, G. A. Voth, P. Salvador, J. J. Dannenberg, S. Dapprich, A. D. Daniels, O. Farkas, J. B. Foresman, J. V. Ortiz, J. Cioslowski, and D. J. Fox, Gaussian, Inc., Wallingford CT, **2009**.

[3] A. D. Becke, *J. Chem. Phys.*, **1993**, *98*, 1372.

[4] C. Lee, W. Yang and R. G. Parr, *Phys. Rev.* B, **1998**, *37*, 785.

[5] Lakshmi, V.; Ravikanth, M. *Dalton Transactions.* **2012**, *41*, 5903.

[6] T. A. Keith and R. F. W. Bader, *Chem. Phys. Lett.*, **1993**, *210*, 223.